

THIS MATERIAL MAY BE PROTECTED BY COPYRIGHT LAW (TITLE 17
U.S. CODE)

Progressive metamorphism of pelitic rocks from protolith to granulite facies, Dutchess County, New York, USA: constraints on the timing of fluid infiltration during regional metamorphism

D. L. WHITNEY,¹ T. A. MECHUM,^{1*} S. M. KUEHNER² AND Y. R. DILEK³

¹Department of Geology, CB #3315, University of North Carolina, Chapel Hill, NC 27599, USA (dwhitney@unc.edu)

²Department of Geological Sciences, AJ-20, University of Washington, Seattle, WA 98195, USA

³Department of Geology and Geography, Vassar College, Poughkeepsie, NY 12601, USA

ABSTRACT A complete Barrovian sequence ranging from unmetamorphosed shales to sillimanite–K-feldspar zone metapelitic gneisses crops out in a region extending from the Hudson River in south-eastern New York state, USA, to the high-grade core of the Taconic range in western Connecticut. NNE-trending subparallel biotite, garnet, staurolite, kyanite, sillimanite and sillimanite–K-feldspar isograds have been identified, although the assignment of Barrovian zones in the high-grade rocks is complicated by the appearance of fibrolitic sillimanite at the kyanite isograd.

Thermobarometric results and reaction textures are used to characterize the metamorphic history of the sequence. Pressure–temperature estimates indicate maximum metamorphic conditions of 475 °C, *c.* 3–4 kbar in the garnet zone to >720 °C, *c.* 5–6 kbar in the highest grade rocks exposed. Some samples in the kyanite zone record anomalous (low) peak conditions because garnet composition has been modified by fluid-assisted reactions.

There is abundant petrographic and mineral chemical information indicating that the sequence (with the possible exception of the granulite facies zone) was infiltrated by a water-rich fluid after garnet growth was nearly completed. The truncation of fluid inclusion trails in garnet by rim growth or recrystallization, however, indicates that metamorphic reactions involving garnet continued subsequent to initial infiltration.

The presence of these textures in some zones of a well-constrained Barrovian sequence allows determination of the timing of fluid infiltration relative to the *P–T* paths. Thermobarometric results obtained using garnet compositions at the boundary between fluid-inclusion-rich and inclusion-free regions of the garnet are interpreted to represent peak metamorphic conditions, whereas rim compositions record slightly lower pressures and temperatures. Assuming that garnet grew during a single metamorphic event, infiltration must have occurred at or slightly after the peak of metamorphism, *i.e.* 4–5 kbar and a temperature of *c.* 525–550 °C for staurolite and kyanite zone rocks.

Key words: Barrovian sequence; Dutchess County, New York; fluid infiltration; metapelitic rocks; thermobarometry.

INTRODUCTION

Barrovian sequences occur throughout the world and contain information about the mineralogical changes experienced by pelitic rocks during regional metamorphism in collisional orogens. Thermobarometric results and petrographic observations can be integrated to characterize the pressure–temperature–reaction history of a progressive metamorphic sequence over many kilometres of crustal thickness. Where there is evidence for synmetamorphic fluid infiltration, this information can be used to constrain the timing and *P–T* conditions of fluid flow.

A progressive metamorphic sequence ranging from

unmetamorphosed sedimentary rocks to sillimanite–K-feldspar zone metapelitic gneisses crops out in Dutchess County, New York, and adjacent regions of western Connecticut, USA (Barth, 1936). The completeness of the sequence and the presence of the likely protoliths of the metamorphic rocks allows a characterization of the geological history from the onset of metamorphism through the granulite facies.

An important issue in petrology and tectonics is the role of fluids in advection of heat and material. The efficiency of fluid-assisted heat and mass transport is in part a function of the temperature and pressure at which fluid flow occurs, and it is therefore of interest to document the *P–T* conditions of fluid flow during metamorphism. The presence of arrested fluid–rock reactions involving garnet and other metamorphic minerals in a Barrovian sequence constrains the timing

*Present address: Department of Geological Sciences, University of Texas – Austin, TX 78713, USA.

of infiltration relative to the P - T paths because inferences from reaction textures can be combined with thermobarometric results.

REGIONAL GEOLOGY

The Dutchess County Barrovian sequence is located in the Taconic Mountains of New York and Connecticut, USA (Fig. 1a). The principal geological formations in the field area include Precambrian gneisses of the Hudson and Housatonic Highlands, the Cambrian Poughquag orthoquartzite (which unconformably overlies the Precambrian gneisses) and Cambrian-Ordovician carbonates (Wappinger, Stockbridge, Inwood Formations) (Fig. 1b). The quartzite, carbonates and associated pelitic rocks represent part of the early Palaeozoic eastern North American shelf sequence (Bence & McLelland, 1976).

The Barrovian sequence is expressed in Ordovician pelitic rocks (Walloomsac Fm, Everett Schist, Manhattan Fm). Protoliths of the metamorphic rocks were probably similar to the east-derived Ordovician turbiditic sandstones and shales (e.g. the Austin Glen and Mt Merino members of the Normanskill Formation) that crop out to the west near the Hudson River (Fig. 1b) and that are part of the Taconic sequence of the Appalachian foreland basin (Drake *et al.*, 1989). Using new age constraints from graptolite zones recognized in Walloomsac shales, Hames *et al.* (1991) proposed that deposition of the shales occurred

at 455–460 Ma, just prior to metamorphism and deformation.

A series of NNE-trending isograds have been mapped (Barth, 1936; Vidale, 1974; present study), with the chlorite zone located in the western part of the section and the sillimanite-K-feldspar isograd c. 30 km to the east (map distance), near the New York and Connecticut border (Fig. 1b). Sutter *et al.* (1985) correlated these isograds with Taconic isograds mapped to the north in Connecticut and Massachusetts.

The geology of the area has been described in detail by Barth (1936) and Balk (1936). Garlick & Epstein (1967) obtained oxygen isotope data for rocks from the garnet through sillimanite zones, and calculated a temperature range of 480–625 °C. Vidale (1974) remapped isograds proposed by Barth (1936) using petrographic rather than field observations of the first appearance of index minerals; this resulted in a slight westward shift of isograds. The most recent published studies of the geology of Dutchess County are field guides by Bence & McLelland (1976), McLelland & Fisher (1976) and Fisher & Warthin (1976), and the geological map of Ratcliffe & Burton (1990). Other studies of the Walloomsac Formation in Connecticut, Massachusetts and New York north of Dutchess County include Wang & Spear (1991) and Hames & Menard (1993).

Metamorphism and deformation occurred during the Taconic (Ordovician) orogeny. Using Rb-Sr and K-Ar whole-rock and mica ages, Long (1962)

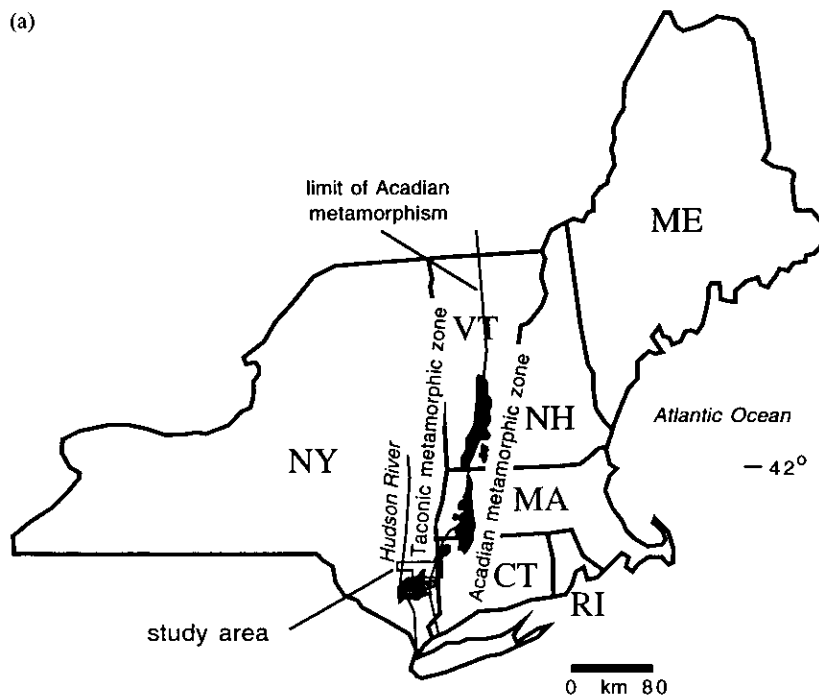
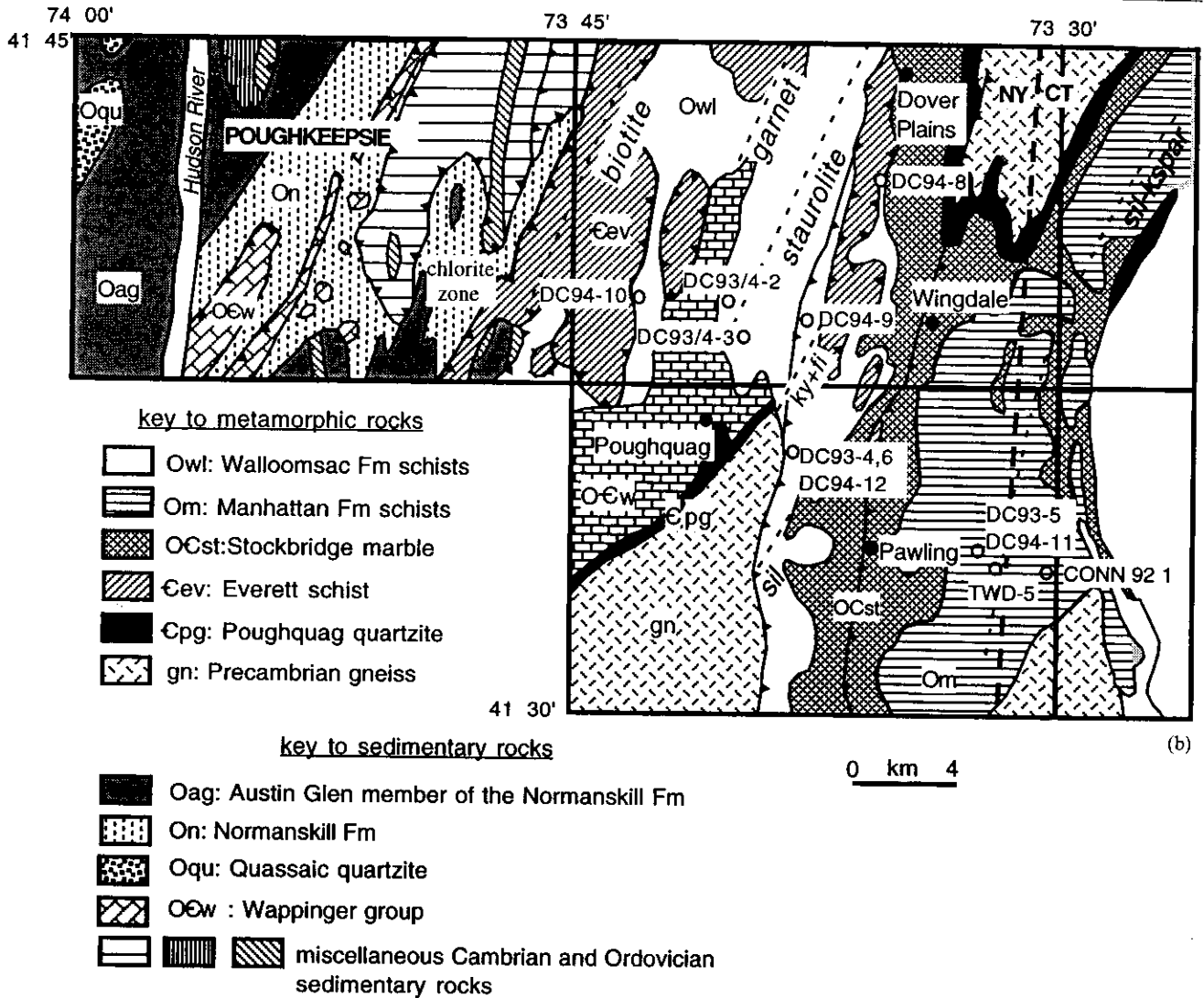


Fig. 1. (a) Regional map showing the location of the study area. The limit of Acadian metamorphism is from Hames *et al.* (1991). (b) Map of Dutchess County with isograds and locations of samples discussed in the text (geology modified from Fisher *et al.*, 1970). Note that the location of the first appearance of kyanite coincides with the first appearance of fibrolitic sillimanite.



determined that the Dutchess County rocks experienced a metamorphic event with a minimum age of 430 Ma (Taconic), and proposed that this had been followed by a lower grade regional thermal event at 360 Ma (Acadian). Bence & Rajamani (1972) obtained $^{40}\text{Ar}/^{39}\text{Ar}$ data for biotite and muscovite from five samples representing various grades, and proposed that the data were consistent with Taconic metamorphism (435 Ma) followed by cooling during uplift, and that the rocks may not have been significantly affected by the Acadian orogeny. Hames *et al.* (1991) used $^{40}\text{Ar}/^{39}\text{Ar}$ dating of micas to determine an age of c. 445 Ma for the Taconic staurolite zone, and delineated an area in which Acadian metamorphism at 390–400 Ma partially overprinted some Taconic textures and mineral rim compositions (Fig. 1a). According to Hames *et al.* (1991), the easternmost part of the Dutchess County sequence may have been affected by Acadian thermal events. Acadian deformation may have affected the region as far west as the Hudson River.

PETROGRAPHY AND MINERAL CHEMISTRY

The mineralogy, textural relations and mineral chemistry of major minerals are described below for the metamorphic rocks, with a brief description of subchlorite zone rocks. The distribution of index minerals in chlorite through sillimanite–K-feldspar zone metapelitic rocks is given in Table 1. General compositional trends apparent across the sequence are (1) an increase in biotite TiO_2 content with grade: TiO_2 increases from c. 1 wt% in low-grade rocks to >3 wt% in sillimanite–K-feldspar zone rocks; (2) an increase in anorthite component in plagioclase from An_{0-7} in the chlorite zone to An_{19-40} in the highest grade rocks; and (3) an increase in paragonite component of muscovite from the chlorite through upper staurolite zone (no muscovite was analysed from the kyanite zone), and a decrease in white mica X_{Na} into the sillimanite–K-feldspar zone. The latter trend is probably the result of increasing solubility of Na in muscovite with increasing temperature, followed by a

Zone	Chl	Bt	Grt	St	Ky	Sil	Sil-Kfs
Chlorite	—————						
Biotite	—————						
Plagioclase*	An ₀₋₆	An ₁₋₁₄	An ₁₂₋₁₈	An ₁₂₋₂₀	An ₂₀₋₂₅	An ₂₁₋₃₀	An ₁₉₋₄₀
Garnet	—————						
Chloritoid	—————						
Staurolite	—————						
Kyanite	—————						
Fibrolitic-Sil	—————						
Sillimanite	—————						
K-feldspar	—————						
Muscovite	Pa _{0.02}	Pa _{0.07}	Pa _{0.07}	Pa _{0.14-19}	Not analysed	Pa _{0.16}	Pa _{0.05}

* Variability in plagioclase composition within zones reflects the presence of several bulk compositions.

Table 1. Mineral distribution in the Dutchess County Barrovian sequence.

Table 2a. Whole-rock major element data, metapelitic rocks.*

Sample Zone	DC94-7 Biotite	DC94-10 Biotite	DC94-2a Garnet	DC94-3 Lower St	DC93-4 Upper St	DC94-8 Upper St	DC94-9 Upper St	DC94-11 Sillimanite
SiO ₂ †	65.01 (0.54)	61.77 (0.34)	63.38 (0.63)	59.57 (0.44)	62.49 (0.23)	60.91 (0.40)	54.18 (0.37)	60.05 (0.37)
TiO ₂	0.80 (0.00)	0.84 (0.00)	0.80 (0.01)	1.01 (0.00)	0.65 (0.00)	0.91 (0.01)	1.29 (0.00)	1.18 (0.01)
Al ₂ O ₃	16.32 (0.11)	18.11 (0.16)	16.43 (0.27)	23.50 (0.34)	14.77 (0.13)	21.34 (0.21)	24.75 (0.22)	23.06 (0.14)
Fe ₂ O ₃ ‡	7.08 (0.06)	8.14 (0.09)	7.33 (0.20)	8.91 (0.20)	6.63 (0.05)	8.99 (0.04)	10.23 (0.06)	7.36 (0.06)
MnO	0.11 (0.00)	0.15 (0.00)	0.14 (0.00)	0.15 (0.00)	0.75 (0.01)	0.16 (0.00)	0.29 (0.00)	0.16 (0.00)
MgO	3.73 (0.73)	4.71 (0.02)	3.87 (0.06)	1.89 (0.02)	8.00 (0.04)	2.11 (0.01)	2.47 (0.02)	1.90 (0.01)
CaO	1.54 (0.02)	0.14 (0.00)	1.87 (0.05)	0.23 (0.01)	1.07 (0.01)	0.29 (0.00)	0.43 (0.01)	0.95 (0.01)
Na ₂ O	0.59 (0.01)	1.40 (0.02)	1.21 (0.03)	1.10 (0.02)	1.61 (0.02)	0.75 (0.01)	1.21 (0.01)	1.18 (0.01)
K ₂ O	3.99 (0.04)	3.76 (0.08)	4.13 (0.20)	3.67 (0.20)	3.92 (0.07)	3.93 (0.03)	4.71 (0.06)	3.33 (0.04)
Total	99.16 (0.66)	99.03 (0.65)	99.15 (1.05)	100.03 (1.14)	99.89 (0.43)	99.40 (0.66)	99.56 (0.62)	99.17 (0.53)
LOI§	4.89	4.70	3.53	3.81	1.46	2.31	2.52	1.80

* Determined by DCP (UNC-Chapel Hill). † Some samples contain quartz veinlets that were impossible to separate from the rest of the rock, and variation in SiO₂ values may reflect their presence. Note, however, that these rocks are not enriched in SiO₂ relative to the average pelites of Ague (1991). ‡ Total Fe expressed as Fe₂O₃. § Loss on ignition.

Table 2b. Whole-rock major element data, subchlorite zone rocks.*

Sample	YD94-1	YD94-2	YD94-3	YD94-4	YD94-5
SiO ₂	66.06	63.15	72.88	65.63	58.42
TiO ₂	0.83	0.78	0.72	0.80	0.94
Al ₂ O ₃	13.24	13.74	12.22	12.83	15.39
FeO†	4.71	5.39	4.53	4.79	6.14
MnO	0.05	0.08	0.04	0.08	0.10
MgO	1.85	2.10	1.62	1.60	2.00
CaO	5.80	6.77	2.45	6.88	8.12
Na ₂ O	1.56	1.77	1.38	1.80	1.62
K ₂ O	2.30	2.35	2.24	2.15	2.85
P ₂ O ₅	0.15	0.14	0.15	0.14	0.16
Total	96.55	96.27	98.23	96.70	95.74

* Determined by XRF (Washington State University). † Total Fe expressed as FeO.

decrease in paragonite component in muscovite owing to breakdown of muscovite + quartz to form plagioclase and Al₂SiO₅. Mg/(Mg + Fe) vs. Al^{VI} in biotite does not appear to correlate with increasing metamorphic grade and may be more a function of differences in protolith bulk composition.

Whole-rock analyses (Table 2) were obtained by DCP spectroscopy (UNC-Chapel Hill) for biotite zone and higher samples, and by XRF (Washington State University) for chlorite and subchlorite zone samples. Mineral analyses were obtained using the Cameca Camebax electron microprobe analyser at Duke University. Representative analyses of six samples (one from each metamorphic zone) selected from a larger suite of samples are given in Tables 3–7. X-ray maps

of garnet used in interpretation of garnet zoning and selection of compositions for thermobarometric calculations were generated with the JEOL 733 electron microprobe at the University of Washington. X-ray intensities were digitized using the GATAN DigitalMicrograph system.

Bulk compositions

Limited whole-rock data (Table 2) for Dutchess County subchlorite through sillimanite zone pelitic rocks reveal that the greatest compositional difference among samples involves variation in Ca (Fig. 2). This probably reflects variation in modal amounts of plagioclase and carbonate. Comparison of Dutchess County metapelitic rocks with average pelitic rock compositions of Ague (1991) indicates that the Dutchess County rocks span a compositional range which encompasses average pelitic major element abundances, but that in general is more enriched in K₂O and depleted in CaO and Na₂O relative to average pelites. The number of analyses is insufficient to detect variation in bulk composition with metamorphic grade.

Despite compositional differences among samples, at least three general bulk compositions can be traced in the pelitic rocks across the entire sequence from low to high grade (Bence & McLelland, 1976). Relatively aluminous, Fe-rich rocks contain chloritoid + chlorite but no biotite in low-grade (biotite zone) rocks. Less

Table 3. Representative muscovite analyses.

Zone	Chlorite	Biotite	Garnet		Staurolite			Sil	Sil-Kfs
	DC93-1 matrix	DC94-7 matrix	DC94-2 matrix	DC94-2 in Bt	DC93-3 matrix	DC94-9 matrix	DC94-9 in Bt	DC93-5 matrix	C 92 1 matrix
SiO ₂	48.41	44.54	46.25	45.84	46.71	46.62	47.09	46.45	45.32
TiO ₂	0.53	0.39	0.11	0.22	0.15	0.18	0.12	0.36	0.53
Al ₂ O ₃	31.12	33.83	36.47	36.40	37.34	36.98	35.56	36.24	36.49
FeO	2.35	3.97	1.24	1.52	1.12	0.78	2.08	2.12	2.98
MnO	<d.l.	<d.l.	<d.l.	0.03	<d.l.	<d.l.	<d.l.	<d.l.	0.02
MgO	2.35	2.77	0.55	0.49	0.67	0.49	1.26	0.45	0.68
CaO	<d.l.	<d.l.	<d.l.	<d.l.	<d.l.	<d.l.	<d.l.	<d.l.	<d.l.
Na ₂ O	0.17	0.47	0.49	0.49	1.01	1.80	1.39	1.24	0.36
K ₂ O	10.23	9.43	10.47	10.58	9.68	9.54	9.71	9.96	10.16
F	0.27	0.14	n.a.	n.a.	n.a.	n.a.	n.a.	n.a.	n.a.
Total	95.43	95.54	95.58	95.57	96.69	96.39	97.21	96.82	96.54
Si	6.43	5.98	6.12	6.09	6.09	6.10	6.15	6.08	6.00
Al ^{IV}	1.57	2.02	1.88	1.91	1.91	1.90	1.85	1.92	2.00
Al ^{VI}	3.30	3.33	3.82	3.79	3.83	3.81	3.63	3.67	3.68
Ti	0.05	0.04	0.01	0.02	0.02	0.02	0.01	0.04	0.05
Fe	0.26	0.45	0.14	0.17	0.12	0.09	0.23	0.23	0.33
Mg	0.47	0.55	0.11	0.10	0.13	0.10	0.25	0.09	0.14
Na	0.04	0.12	0.12	0.13	0.26	0.38	0.35	0.32	0.09
K	1.73	1.62	1.77	1.79	1.61	1.63	1.62	1.66	1.72
X _{Na}	0.02	0.07	0.06	0.07	0.14	0.19	0.18	0.16	0.05

* Cations calculated on a 22-oxygen basis.

Table 4. Representative plagioclase compositions.

Zone	Biotite	Garnet	Lower staurolite		Upper staurolite				Kyanite		Sillimanite		Sil-Kfs	
	DC94-7	DC94-2	DC93-3 core	DC93-3 rim	DC94-9 core	DC94-9 rim	DC94-9 incl. core	DC94-9 incl. rim	DC93-4 core	DC93-4 rim	DC93-5 core	DC93-5 rim	C 92 1 core	C 92 1 rim
SiO ₂	66.41	56.93	65.31	65.24	63.93	64.13	61.53	61.30	61.92	61.75	61.13	61.21	65.42	64.75
Al ₂ O ₃	21.46	27.57	22.02	22.26	23.11	22.81	23.88	24.67	23.79	23.90	24.82	24.38	22.88	23.16
FeO	0.18	0.03	0.02	0.06	0.10	0.06	0.17	0.39	0.06	0.11	0.03	0.31	<d.l.	<d.l.
CaO	1.53	9.17	2.67	3.01	3.61	3.83	4.98	6.65	5.27	5.26	5.45	4.90	3.51	3.62
Na ₂ O	10.50	6.25	10.32	10.19	9.35	9.35	8.95	7.20	9.02	8.97	8.61	8.90	8.14	7.94
K ₂ O	0.06	0.04	0.03	0.05	0.04	0.03	0.03	0.05	0.05	0.05	0.06	0.13	0.17	0.22
Total	100.14	99.99	100.37	100.81	100.14	100.21	99.54	100.26	100.10	100.04	100.10	99.83	100.12	99.69
Si	2.91	2.55	2.86	2.85	2.81	2.82	2.74	2.71	2.75	2.74	2.71	2.72	2.86	2.84
Al	1.11	1.46	1.13	1.15	1.20	1.18	1.25	1.29	1.24	1.25	1.29	1.28	1.18	1.20
Fe	0.06	0.00	0.00	0.00	0.00	0.00	0.00	0.01	0.00	0.00	0.00	0.01	0.00	0.00
Ca	0.07	0.44	0.12	0.14	0.17	0.18	0.24	0.32	0.25	0.25	0.26	0.23	0.16	0.17
Na	0.89	0.54	0.88	0.86	0.80	0.80	0.77	0.62	0.78	0.77	0.75	0.77	0.69	0.68
K	0.00	0.00	0.00	0.00	0.00	0.00	0.00	0.00	0.00	0.00	0.00	0.01	0.01	0.01
X _{Na}	0.07	0.45*	0.12	0.14	0.18	0.18	0.23	0.34	0.24	0.24	0.26	0.23	0.19	0.20

* The composition of plagioclase in this rock is unusually anorthitic for the garnet zone.

aluminous shales are metamorphosed to pelitic phyl-lites and schists that contain biotite + chlorite, and are more graphitic than the aluminous rocks. Siliceous (sandy) protoliths are represented in the Barrovian sequence by quartz-rich and relatively mica-poor, massive rocks. Mineralogical differences in biotite zone and higher rocks make it possible to distinguish among these bulk compositions that probably represent different sedimentary layers in the original turbiditic protoliths (cf. Bence & McLelland, 1976).

Subchlorite and chlorite zones

Unmetamorphosed to incipiently metamorphosed sil-iclastic rocks of the Austin Glen member of the Normanskill Formation and its equivalents in the vicinity of the Hudson River consist of alternating layers of sandstone, siltstone and shale that display

centimetre-scale to 1-m-thick bedding. Millimetre-scale layering is apparent within the shale beds. East of the Hudson River, the sedimentary rocks are gently folded around axes that generally trend to the NE and that plunge moderately to the NE. Primary structures, ripple marks and shell fragments are well preserved. Bedding-parallel cleavage is locally developed, and a moderately well-developed fracture cleavage is perpendicular to bedding and subparallel to the axial plane of the gentle folds.

Further east in the same formation, the sandstone-siltstone-shale package displays open to close folds with similar orientation, and the fracture cleavage becomes more prominent. Bedding-parallel cleavage planes display random mica flakes. Dark red and green-coloured Normanskill Formation chert and siliceous shale units in the chlorite zone are tightly to isoclinally folded and show crenulation cleavage with SW-

Table 5. Representative biotite analyses.

Zone	Biotite		Garnet		Lower staurolite		Upper staurolite		Kyanite		Sillimanite		Sil-Kfs	
	DC94-7 matrix	DC94-2 matrix	DC94-2 nr Grt	DC93-3 matrix	DC93-3 nr Grt	DC94-9 matrix	DC94-9 nr Grt	DC93-4 matrix	DC93-4 nr Grt	DC93-5 matrix	DC93-5 nr Grt	C 92 1 matrix	C 92 1 nr Grt	
SiO ₂	36.26	35.79	34.56	35.84	36.27	35.63	35.72	40.46	39.82	35.17	34.84	34.36	33.95	
TiO ₂	1.36	1.07	1.00	1.65	1.81	1.22	1.32	1.11	1.06	1.98	1.56	3.01	3.62	
Al ₂ O ₃	18.98	19.42	19.29	20.06	19.66	20.37	20.21	19.88	19.72	18.64	19.17	19.25	18.64	
FeO	17.92	22.81	22.23	22.28	21.47	19.31	20.02	10.01	10.46	24.46	24.59	22.10	22.01	
MnO	0.09	0.05	0.06	<d.l.	<d.l.	0.04	0.04	0.14	0.20	0.01	0.01	0.32	0.23	
MgO	11.55	8.62	8.45	8.78	8.67	10.85	10.83	17.62	17.63	7.76	7.73	8.13	8.29	
CaO	0.02	<d.l.	0.02	0.02	<d.l.	<d.l.	<d.l.	<d.l.	<d.l.	<d.l.	0.02	<d.l.	<d.l.	
Na ₂ O	0.13	0.14	0.10	0.20	0.19	0.26	0.21	0.35	0.41	0.27	0.23	0.05	0.06	
K ₂ O	9.32	9.72	9.27	8.21	8.18	10.11	9.83	7.52	7.69	9.55	9.29	9.66	9.66	
F	0.55	n.a.	n.a.	n.a.	n.a.	0.21	0.17	n.a.	n.a.	0.61	0.42	n.a.	n.a.	
Cl	0.01	n.a.	n.a.	n.a.	n.a.	<d.l.	<d.l.	n.a.	n.a.	<d.l.	<d.l.	n.a.	n.a.	
Total	96.19	97.62	94.98	97.04	96.26	98.01	98.35	97.09	96.99	98.45	97.86	96.88	96.46	
Si	5.38	5.34	5.39	5.37	5.45	5.28	5.27	5.65	5.59	5.27	5.27	5.24	5.21	
Al ^{IV}	2.62	2.60	2.61	2.63	2.55	2.72	2.73	2.35	2.41	2.72	2.73	2.76	2.79	
Al ^{VI}	0.70	0.85	0.90	0.91	0.94	0.80	0.79	0.92	0.86	0.57	0.68	0.69	0.57	
Ti	0.15	0.12	0.12	0.19	0.21	0.14	0.15	0.12	0.11	0.22	0.18	0.34	0.42	
Fe	2.22	2.88	2.87	2.79	2.70	0.39	2.47	1.17	1.23	3.07	3.11	2.82	2.82	
Mn	0.01	0.01	0.01	0.00	0.00	0.00	0.01	0.02	0.02	0.00	0.00	0.04	0.03	
Mg	2.56	1.94	1.91	1.96	1.94	2.40	2.38	3.67	3.69	1.74	1.74	1.85	1.89	
Na	0.00	0.04	0.45	0.06	0.05	0.07	0.06	0.09	0.11	0.08	0.07	0.02	0.02	
K	1.76	1.87	1.85	1.57	0.93	1.91	1.85	1.34	1.38	1.83	1.79	1.88	1.89	
X _{Fe}	0.39	0.50	0.51	0.48	0.47	0.42	0.43	0.20	0.21	0.55	0.54	0.49	0.49	
X _{Mg}	0.45	0.34	0.34	0.34	0.34	0.42	0.41	0.62	0.62	0.31	0.31	0.32	0.33	
X _{Ti}	0.03	0.02	0.03	0.03	0.04	0.02	0.03	0.02	0.02	0.10	0.03	0.06	0.10	
X ^{VI} _{vt}	0.12	0.15	0.13	0.16	0.16	0.14	0.14	0.16	0.15	0.04	0.12	0.12	0.07	

* Cations calculated on a 22-oxygen basis. n.d. = not determined. <d.l. = less than detection limit.

Table 6. Representative garnet analyses.

Zone	Garnet		Lower staurolite		Upper staurolite		Kyanite		Sillimanite		Sil-Kfs	
	DC94-2 core	DC94-2 rim	DC93-3 core	DC93-3 rim	DC94-9 core	DC94-9 rim	DC93-4 core	DC93-4 rim	DC93-5 core	DC93-5 rim	C 92 1 core	C 92 1 rim
SiO ₂	37.90	36.98	36.66	36.69	36.48	37.09	37.58	37.63	37.06	37.00	36.66	36.73
TiO ₂	0.07	0.04	0.08	0.02	0.09	0.02	0.10	<d.l.	<d.l.	0.04	0.02	0.02
Al ₂ O ₃	20.89	20.93	20.35	20.69	20.56	20.44	21.36	21.23	20.39	20.24	21.12	21.00
FeO	26.08	34.07	30.09	38.26	30.04	35.77	18.64	20.91	38.60	38.93	26.02	26.96
MnO	10.42	4.22	8.48	0.83	5.97	2.89	15.09	14.29	1.01	0.08	12.11	11.67
MgO	0.81	1.41	0.81	1.89	1.34	2.53	3.43	3.87	2.05	2.03	2.49	2.55
CaO	3.72	2.62	3.48	1.72	5.15	1.62	3.34	1.70	1.55	2.14	0.83	0.90
Total	99.89	100.27	99.95	100.10	99.63	100.36	99.54	99.63	100.66	100.46	99.25	99.83
Si	3.06	3.00	3.00	3.00	2.98	3.00	3.00	3.01	3.00	3.01	2.99	2.98
Ti	0.00	0.00	0.01	0.00	0.01	0.00	0.01	0.00	0.00	0.00	0.00	0.00
Al	1.99	2.00	1.96	1.99	1.98	1.95	2.01	2.00	1.95	1.94	2.00	2.01
Fe	1.76	2.31	2.06	2.61	2.05	2.42	1.25	1.40	2.62	2.64	1.82	1.83
Mn	0.71	0.29	0.58	0.06	0.41	0.20	1.02	0.99	0.07	0.01	0.82	0.80
Mg	0.10	0.17	0.10	0.23	0.16	0.31	0.45	0.46	0.25	0.25	0.30	0.31
Ca	0.32	0.23	0.31	0.15	0.45	0.14	0.20	0.15	0.13	0.19	0.07	0.08
X _{alm}	0.61	0.77	0.68	0.86	0.67	0.79	0.42	0.47	0.85	0.86	0.61	0.61
X _{sp}	0.25	0.10	0.19	0.02	0.13	0.07	0.35	0.33	0.02	0.00	0.27	0.27
X _{prp}	0.03	0.06	0.03	0.08	0.05	0.10	0.14	0.16	0.08	0.08	0.10	0.10
X _{grs}	0.11	0.08	0.10	0.05	0.15	0.05	0.10	0.05	0.04	0.06	0.02	0.03

Note: rim and outer core compositions are used in thermobarometric calculations.

plunging crenulation lineations. Principal minerals in the chlorite zone phyllites are chlorite, white mica, plagioclase, quartz, ilmenite and graphite ± carbonate. White mica is phengitic (Table 3), plagioclase is nearly pure albite (Table 4) and chlorite is relatively aluminous (cf. Bence & McLelland, 1976).

Biotite zone

Biotite zone graphitic phyllites contain large biotite (Table 5) and Fe-Mn ilmenite porphyroblasts in a fine-grained matrix of white mica, chlorite, graphite and ankerite. White mica is phengitic (Table 3) and

Table 7. Representative chloritoid and staurolite analyses.

Zone	Staurolite		Sillimanite	Staurolite	
	DC93-3 St in Cld	DC94-9 St-rim*	DC94-11 St-rim*	DC93-3 Cld-core	DC93-3 Cld-rim
SiO ₂	28.49	28.97	28.14	24.18	24.33
TiO ₂	0.26	0.48	0.50	0.01	0.02
Al ₂ O ₃	54.27	53.82	54.63	39.10	39.55
FeO	13.20	14.15	14.28	25.13	24.86
MnO	0.04	0.14	0.01	0.10	0.06
MgO	1.11	1.61	1.51	2.18	2.35
CaO	<d.l.	<d.l.	<d.l.	<d.l.	<d.l.
Total	97.37	99.17	99.06	90.70	91.17
	48 ox.	48 ox.	48 ox.	12 ox.	12 ox.
Si	2.06	2.01	2.01	2.05	2.04
Ti	0.01	0.03	0.03	0.00	0.00
Al	4.62	4.53	4.60	3.90	3.91
Fe	0.80	0.84	0.85	1.78	1.75
Mn	0.00	0.01	0.00	0.01	0.01
Mg	0.12	0.17	0.16	0.28	0.30
X _{Fe}	0.87	0.83	0.84	0.86	0.85

* Unzoned.

plagioclase is albitic (An₀₇; Table 4). Aluminous layers contain chloritoid rather than biotite.

Garnet zone

Garnet zone rocks contain layers that range from quartz-rich to extremely mica- and graphite-rich on an outcrop scale (Fig. 3). These differences in bulk composition and modal mineralogy occur on a scale similar to those observed in the inferred protoliths to the west.

Quartz-rich samples are massive in outcrop and contain small (<0.5 mm), partially resorbed garnet and very fine-grained green biotite in a matrix dominated by quartz (>70 modal %). Some garnet grains retain idiomorphic crystal faces, whereas other grains in the same thin section are anhedral and surrounded by mosaic-textured quartz that is coarser than quartz in the rest of the groundmass (Fig. 3d). The most resorbed garnet grains are located in or near quartz veins. Garnet in the quartz-rich rocks is Mn-rich (X_{sps} up to 0.20; Table 6).

Graphitic phyllites contain abundant, large (1 mm), idiomorphic garnet (Fig. 3a), biotite and ilmenite porphyroblasts, and a matrix of fine-grained chlorite, muscovite, quartz and graphite with accessory tourmaline, pyrite and zircon. Garnet is normally zoned (Fig. 3b), with Fe,Mn-rich cores (X_{alm}=0.61; X_{sps}=0.20-0.25) where X_{alm} >> X_{sps} > X_{grs} > X_{prp}. Garnet rim regions are also Fe-rich (X_{alm}=0.75-0.80), but are Mn-, Mg- and Ca-poor (Table 6).

Biotite in garnet zone rocks is relatively low in Ti compared to higher grade rocks (Table 5). Biotite has overgrown a foliation defined in part by graphite, and the biotite grains were subsequently kinked, resulting in clear (graphite-free) kink-bands. Muscovite contains less Fe and Mg than the white mica in chlorite and biotite zones (Table 3).

Plagioclase is fine grained, untwinned and relatively sodic (An₁₃). Grains are essentially homogeneous (Table 4).

Both pelitic and quartz-rich lithologies are cross-cut

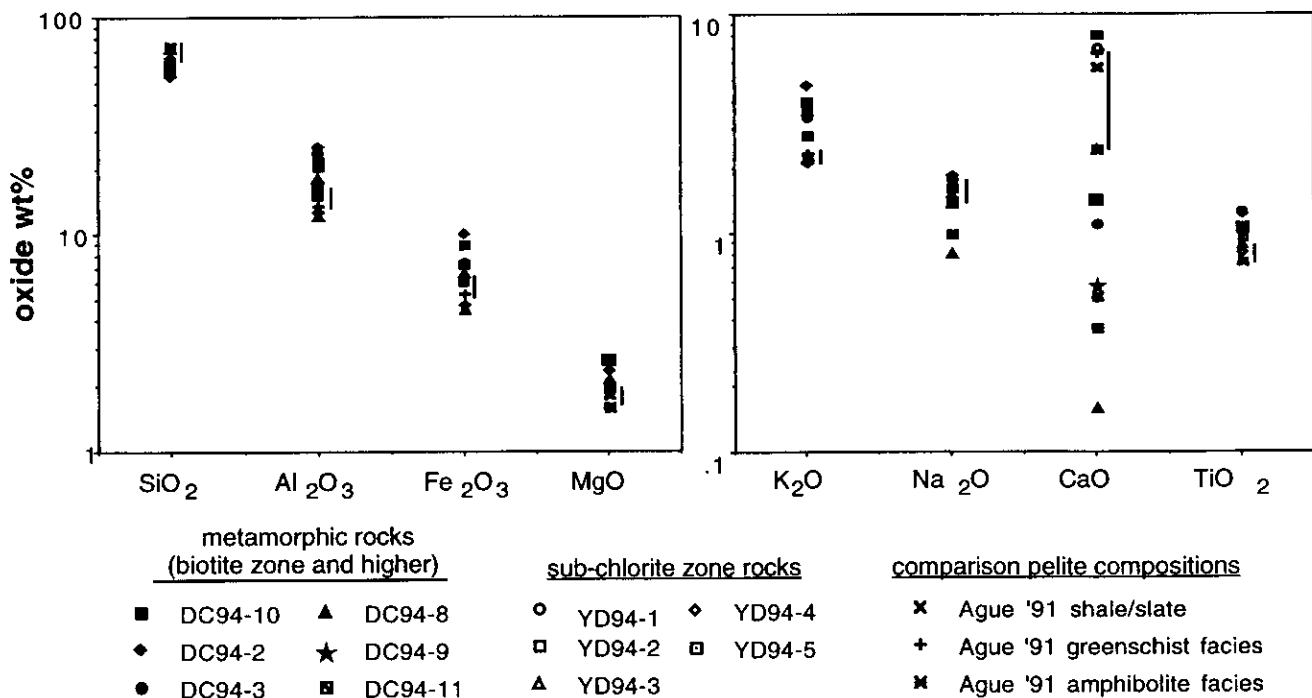


Fig. 2. Whole-rock major element chemistry of Dutchess County metapelitic rocks (subchlorite zone through sillimanite zone; Table 2). Compositions of average pelites from Ague (1991) – highlighted by vertical lines to right of symbols – are shown for comparison. Most of the subchlorite zone samples were collected from the Normanskill Fm north of the map area in Fig. 1(b).

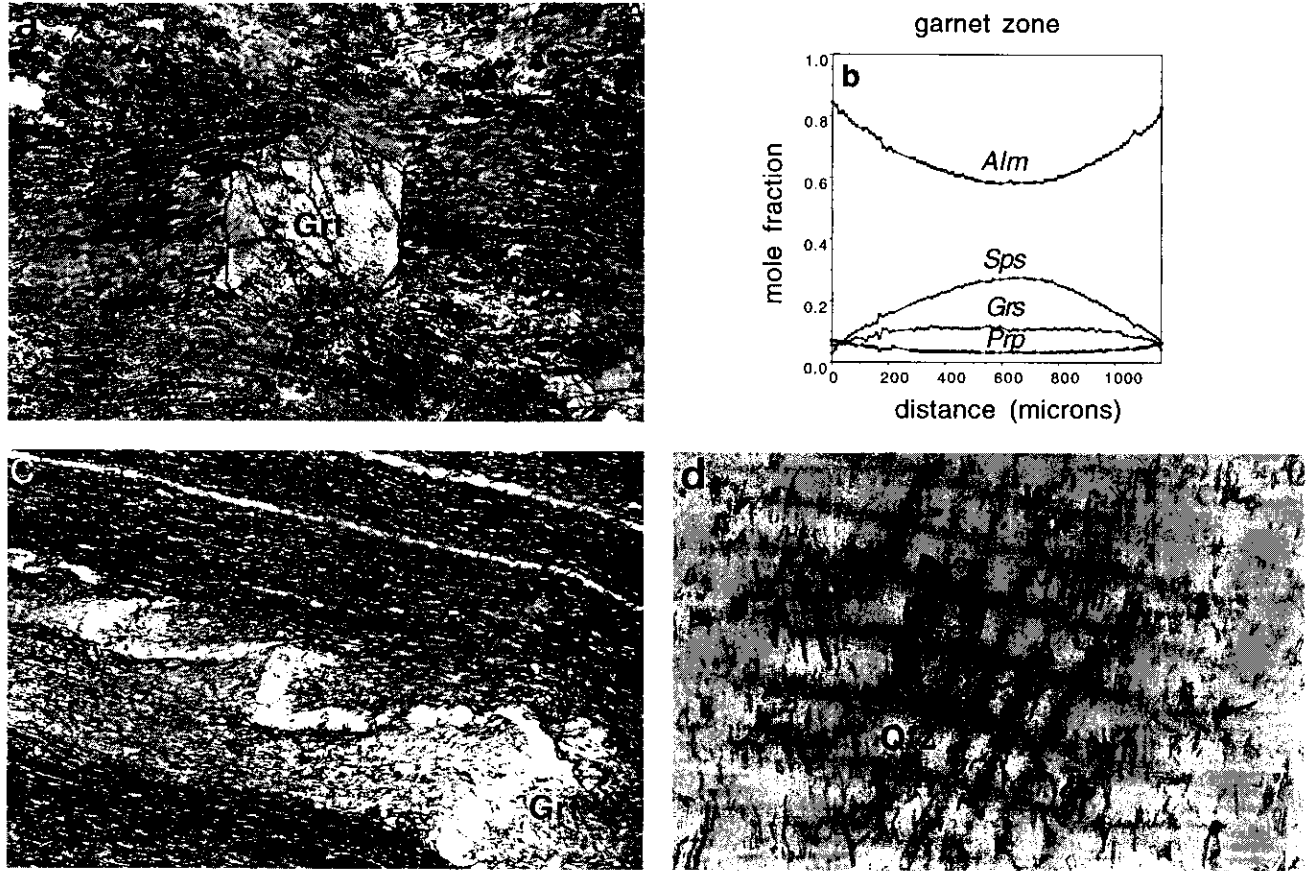


Fig. 3. Garnet zone. (a) Typical idiomorphic garnet in a matrix of biotite, chlorite, muscovite, quartz, graphite, plagioclase and ilmenite. Field of view = 2.75 mm. (b) Growth zoning; alm = almandine, grs = grossular; prp = pyrope; sps = spessartine. (c) Ptygmatically folded quartz vein in layered phyllite. Note the garnet that has been truncated by a vein. Field of view = 2.75 mm. (d) Resorbed garnet in quartz-rich rock; the garnet is surrounded by a mosaic of recrystallized quartz. Field of view = 1.5 mm.

by millimetre-scale veins containing highly recrystallized aggregates of quartz and fine-grained fibres of chlorite. These veins, which truncate garnet and biotite, are ptygmatically folded (Fig. 3c).

Staurolite zone

Most staurolite zone rocks in Dutchess County contain the assemblage garnet + biotite + muscovite + staurolite + quartz + plagioclase + ilmenite + graphite \pm chloritoid \pm tourmaline. The staurolite zone can be divided into lower and upper zones. Lower staurolite zone samples are phyllites collected close to the staurolite-in isograd and contain chloritoid in Fe-rich, aluminous rocks. Upper zone rocks crop out further to the east and do not contain chloritoid.

In lower staurolite zone aluminous phyllites, idiomorphic garnet (1–2 mm diameter) has partially overgrown and is embayed by chloritoid ($X_{\text{Fe-cld}} = 0.85$) and ilmenite. Chloritoid and ilmenite grains that are partially included in garnet are bent at the garnet-matrix boundary (Figs 4a & 5b). The part of the ilmenite or chloritoid extending into the matrix is in the plane of the foliation defined by micas + graphite

and quartz segregations (Fig. 5a,b). Large tabular grains of chloritoid in the matrix are randomly orientated and overgrew this foliation (Fig. 5a; Table 7). Although most ilmenite grains are orientated parallel to the foliation defined by micas, some grains are orientated at a steep angle to the foliation.

Idiomorphic staurolite is present in the matrix as well as inside chloritoid ($X_{\text{Fe-str}} = 0.87$; Fig. 4d, Table 7). Texturally late chlorite occurs around staurolite in chloritoid and in fractures in these minerals. Grain boundaries between matrix staurolite and garnet are straight.

Some upper staurolite zone rocks contain large (c. 1 cm long) poikiloblastic staurolite and biotite porphyroblasts. The staurolite grains have overgrown a crenulated foliation and partially or completely surround idiomorphic garnets. Garnet inclusions contain elongate quartz, tourmaline and ilmenite inclusions that define an internal fabric that is concordant with the internal foliation in the host staurolite, although the crenulations are not as tightly folded in garnet (Fig. 6a).

There are no significant differences in garnet composition between the lower and upper staurolite

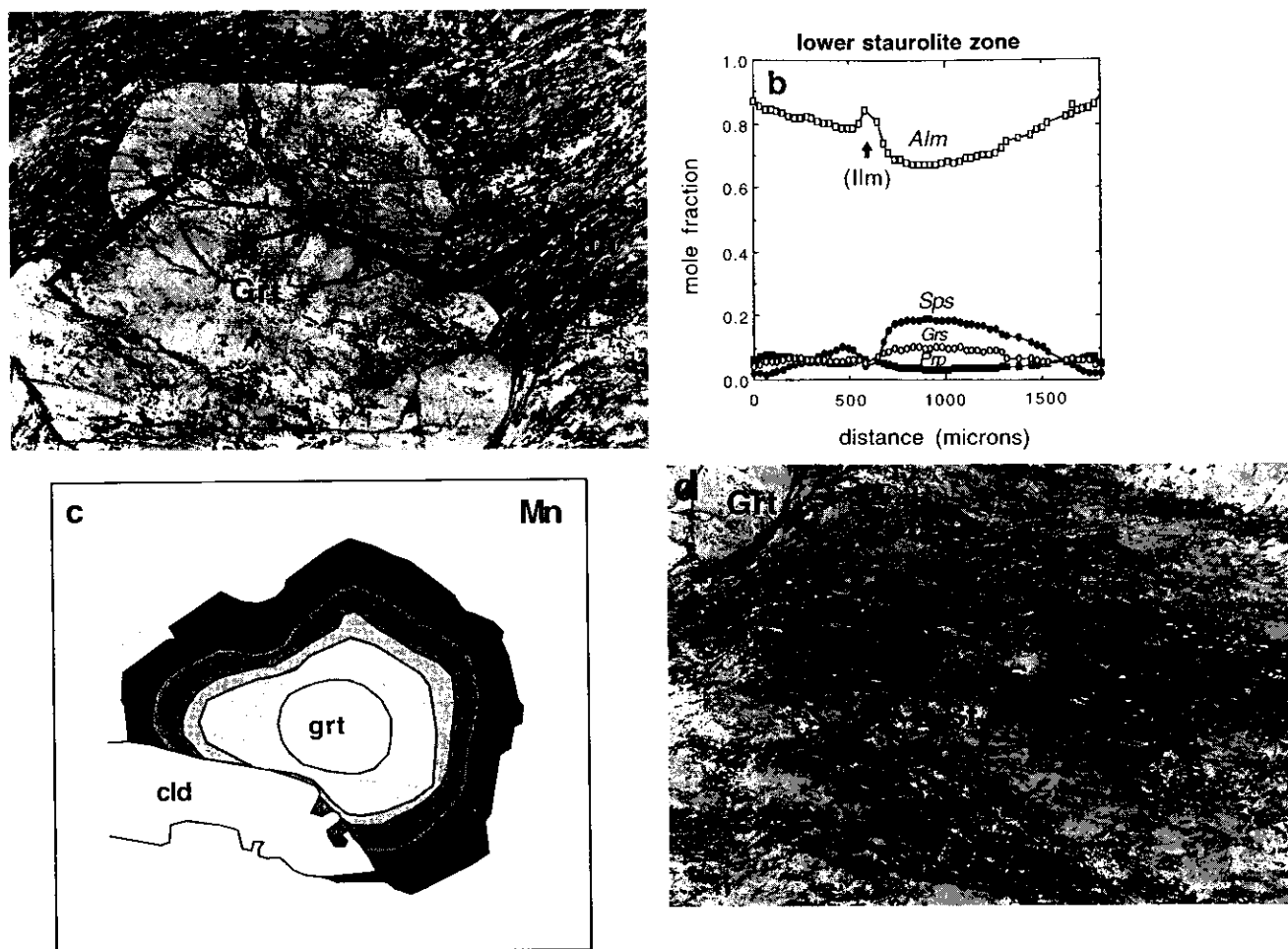


Fig. 4. Lower staurolite zone. (a) Photomicrograph of garnet with folded, partially included ilmenite grain (see text for discussion). Note resorption of garnet rim in the vicinity of ilmenite. Field of view = 2.75 mm. A colour X-ray map of the Mn zoning in the garnet can be assessed through the WWW home page of the journal or directly at URL <http://www.gly.bris.ac.uk/www/jmg/1996/14212-F4a.gif>. (b) Zoning profile of the garnet shown in (a). The local increase in Fe and decrease in Mn is related to the presence of the ilmenite grain on the right hand side of the photograph. (c) Cartoon of concentric Mn growth zoning in garnet (highest Mn concentration in the centre of the grain). The figure was generated by sketching over an X-ray map with well-defined compositional zones. Zoning is truncated by the chloritoid grain. A colour X-ray image is available at URL: <http://www.gly.bris.ac.uk/www/jmg/1996/14212-F4c.gif>. (d) Idiomorphic staurolite in chloritoid. Field of view = 2.75 mm.

zone (Table 6). Garnet is almandine-rich ($X_{alm} = 0.67$, core; 0.78–0.86, rim), with $X_{alm} \gg X_{sps} > X_{grs} > X_{prp}$ in garnet cores, and $X_{alm} > X_{prp} = X_{grs} > X_{sps}$ at the rim (Figs 4b & 6b). Garnet included in staurolite has similar compositions and zoning patterns to matrix garnet. Retrograde zoning at the rim affects the outer 40 μm . Garnet exhibits normal growth zoning, but zoning has been truncated and disrupted in those garnet grains embayed by chloritoid (Fig. 4c). Where chloritoid embays garnet, almandine increases (ΔX_{alm} c. 0.11) and spessartine decreases (ΔX_{sps} c. 0.04). Pyrope and grossular are essentially unchanged near chloritoid. In the vicinity of ilmenite inclusions, garnet composition changes from X_{alm} c. 0.70–75 to 0.84 and X_{sps} from 0.04 to 0.09–0.18 over a distance of 150 μm (Fig. 4b). The magnitude of increase or decrease of components in garnet around ilmenite inclusions is not symmetric on either side because zoning around

the inclusions is superimposed on pre-existing growth zoning (Fig. 4b).

Plagioclase in staurolite zone metapelites is in the range An_{12-18} , with the more calcic compositions in the upper staurolite zone rocks (Table 4). Grains are essentially homogeneous, although some are slightly irregularly zoned. Plagioclase inclusions in garnet are zoned, with anorthite content increasing from core to rim. Typical values for apparent plagioclase core to rim ΔX_{An} are c. 0.05–0.10, although one large inclusion is symmetrically zoned from pure albite in the core to An_{35} at the rim. Garnet composition decreases in Ca and Mn and increases in Fe and Mg in the vicinity of reverse zoned plagioclase inclusions (cf. Whitney, 1991).

Staurolite zone rocks contain abundant quartz veins containing accessory plagioclase + apatite + white mica. These veins cross-cut and truncate garnet, and there is a thin (100–150 μm) texturally and compositionally

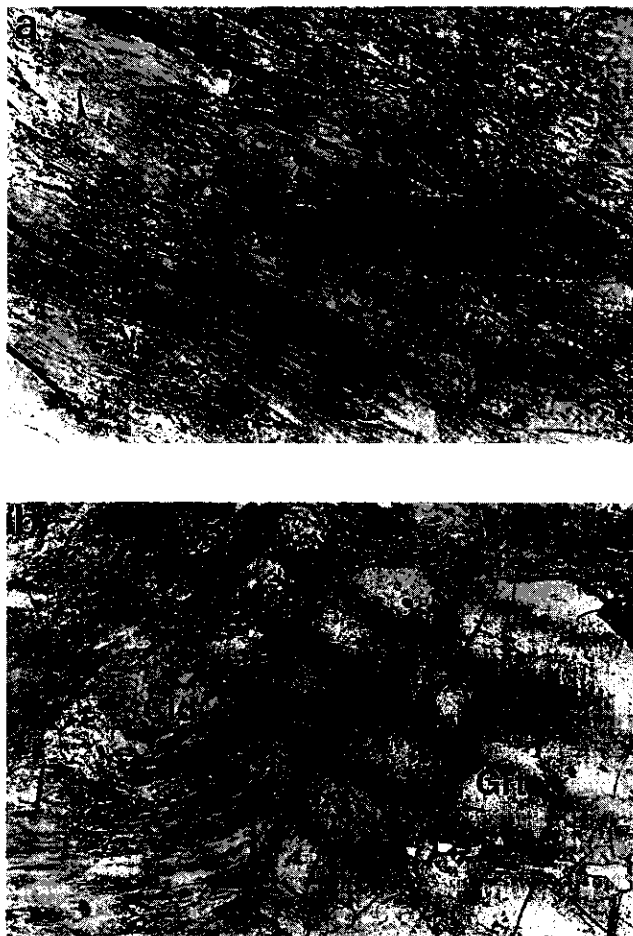


Fig. 5. Lower staurolite zone. (a) Chloritoid grains growing across a pre-existing foliation defined by micas. Grey areas in the chloritoid correspond to where the crystal has overgrown a graphite-rich area; clear areas overgrew quartz-rich regions. Field of view = 2.75 mm. (b) Chloritoid partially included in garnet. Field of view = 2.75 mm.

modified zone in garnet along the vein–garnet contact (Fig. 6d) (Whitney *et al.*, in press). These zones contain no quartz inclusions, although the rest of the garnet contains abundant quartz inclusions, and are clouded by fluid inclusions, some of which are confined to pseudosecondary trails orientated perpendicular to the trend of the adjacent vein (Fig. 6d). Garnet growth zoning is truncated and perturbed in the vicinity of the veins (Whitney *et al.*, in press).

Kyanite zone

Most kyanite-bearing metapelitic rocks in Dutchess County contain the assemblage garnet + biotite + muscovite + quartz + plagioclase + kyanite ± staurolite + ilmenite ± rutile. Many kyanite-bearing samples contain trace amounts of fibrolitic sillimanite along kyanite rims and associated with biotite. Some centimetre-scale layers are extremely fine grained and contain biotite + plagioclase + quartz + (rare) garnet + fibrolitic

sillimanite but no kyanite. These layers are adjacent to centimetre- to decimetre-thick layers containing abundant garnet and large kyanite blades + trace fibrolitic sillimanite.

Kink-folded, 1-cm-long kyanite blades appear blue in hand sample and contain inclusions of rutile, quartz, biotite, apatite, muscovite and idiomorphic garnet. The garnet inclusions contain trails of mineral inclusions (primarily quartz) orientated at a steep angle to the matrix foliation defined by alignment of micas and the host kyanite. Garnet included in kyanite has the same compositions and zoning patterns as matrix garnet. Internal fabrics in both matrix and inclusion garnet in the same thin section have the same orientation.

In some samples, garnet is locally embayed, with plagioclase ± fibrolite filling the embayments (Fig. 7a). Where garnet is not embayed, biotite is adjacent to the garnet rim.

Garnet contains inclusions of quartz, biotite, plagioclase, tourmaline, rutile, Fe–Mn ilmenite, muscovite and zircon. Plagioclase inclusions in garnet are slightly reverse zoned, and grossular in garnet decreases slightly in the vicinity of plagioclase inclusions.

Kyanite zone garnet contains abundant, minute mineral and fluid inclusions (Figs 7 & 8). The mineral inclusions are difficult to identify because of their small size, but some resemble apatite and graphite. Fluid inclusions occur in several textural varieties: (1) a series of parallel pseudosecondary trails extending across garnet (Fig. 7a), with no consistent orientation among all garnets in a thin section; (2) associated with visible fractures in garnet interiors; (3) in trails in near-rim regions in grains that are adjacent to quartz veins (Fig. 6d); (4) as random arrays clouding garnet interiors (i.e. not in visible trails; Fig. 7c); and (5) in arrays radiating from the garnet core (Figs 7d & 8).

Garnet adjacent to veins shows similar features to those described above for upper staurolite zone samples, i.e. fluid-inclusion-filled zones adjacent to the veins, and disrupted growth zoning patterns. Some veins contain quartz + plagioclase, but others are essentially monomineralic quartz. Most veins are pygmatically folded.

Near-rim regions of garnet not adjacent to quartz veins are inclusion-free, and this inclusion-free zone follows the outline of the garnet rim, even around embayments (Fig. 7a,c). There are also inclusion-free zones surrounding mineral inclusions such as quartz and biotite in garnet (Fig. 7c), although the region immediately outside this clear zone may be a site of higher concentration of inclusions than in the rest of the garnet. More detailed observations are presented in Whitney *et al.* (in press), who interpret these features as evidence for open-system net transfer reactions in garnet interiors involving dissolution and reprecipitation of garnet during high-grade metamorphism.

Some matrix garnet contains a nearly homogeneous region in the core (*c.* 500–600 μm in diameter) but displays normal growth zoning from the outer part of

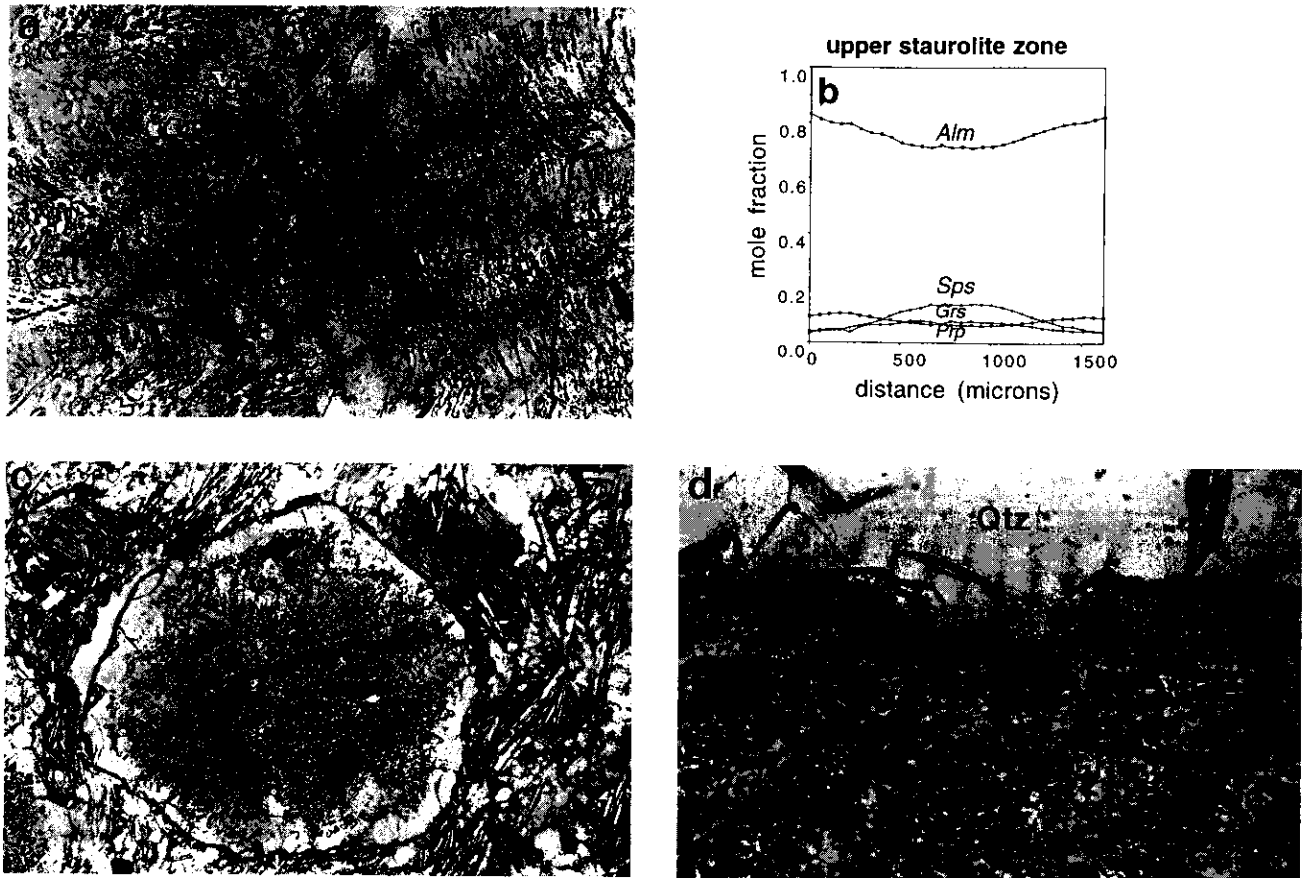


Fig. 6. Upper staurolite zone. (a) Photomicrograph of a large garnet inclusion in staurolite. Garnet and staurolite overgrew a crenulation fabric defined by quartz and ilmenite. Field of view = 2.75 mm. (b) Garnet growth zoning. (c) Garnet in the matrix of a muscovite-rich sample. The large clear inclusions in garnet are reverse-zoned plagioclase inclusions. (d) Garnet from the same sample as (c) exhibiting a reaction texture along the contact with a quartz vein. The minute inclusions in the garnet near the vein are fluid inclusions. Note the absence in this zone of quartz inclusions that are ubiquitous in the rest of the garnet. Field of view = 1.5 mm.

this homogeneous core to the rim with $X_{alm} \geq X_{sps} > X_{grs} \geq X_{prp}$ in garnet core regions, and $X_{alm} \gg X_{sps} > X_{prp} > X_{grs}$ in near-rim regions. Some garnet is extremely spessartine-rich, e.g. $X_{sps} = 0.38$ (core) and 0.33 (rim) (Table 6; Fig. 7b).

The boundary between the inclusion-rich core and inclusion-free rim regions described above corresponds to a slight discontinuity in zoning: X_{alm} continues to increase, but the concentration profiles steepen towards the rim; X_{sps} is homogeneous in some garnet grains and increases in others; X_{grs} decreases; and X_{prp} is homogeneous in some garnet grains and decreases towards the rim in others. Growth zoning in garnet adjacent to veins has been significantly perturbed compared to normal growth zoning (Whitney *et al.*, in press).

Sillimanite zone

As noted above, the first appearance of sillimanite (fibrolite) coincides with the kyanite-in isograd. The sillimanite zone is defined as the region containing

abundant fibrolitic sillimanite and rare, prismatic sillimanite. Relict kyanite and staurolite persist in some samples. Sillimanite zone metapelitic schists also contain garnet + biotite + muscovite + quartz + plagioclase + sillimanite/fibrolitic sillimanite + ilmenite ± staurolite ± kyanite + tourmaline. Calcisilicates inter-layered with the metapelitic rocks contain calcite + tremolite + diopside + phlogopite.

Staurolite in sillimanite zone samples is typically irregularly shaped and disaggregated. Some staurolite porphyroblasts are surrounded by a thick envelope of biotite. Staurolite grains have sharp contacts with garnet, but are partially replaced by fibrolitic sillimanite along rims and cracks. Inclusions of staurolite are present in garnet and muscovite, and staurolite itself contains idiomorphic garnet inclusions.

Some samples contain abundant mats of fibrolitic sillimanite (up to 10–15 modal %) as well as randomly orientated fibrolitic sillimanite sprays in quartz, plagioclase and muscovite, and patches of fibrolitic sillimanite in quartz inclusions in garnet (Fig. 9a). Relic staurolite and kyanite are present in this rock, and fibrolitic

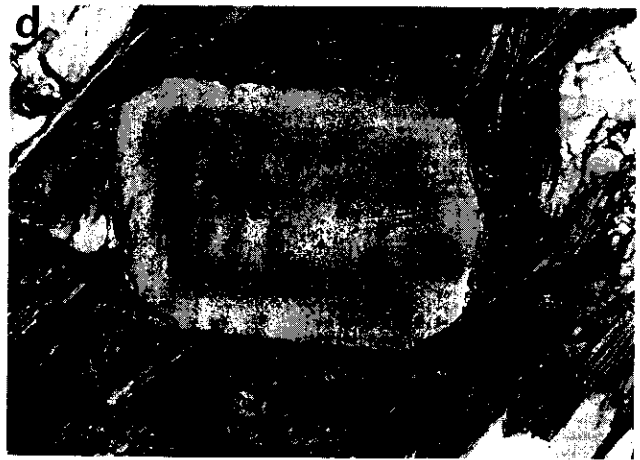
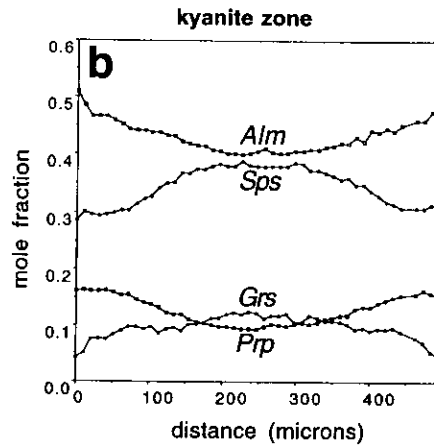


Fig. 7. Kyanite zone. (a) Garnet containing arrays of pseudosecondary fluid inclusions. Note the clear zone in the garnet near-rim region that follows the outline of the garnet, even around embayments. Embayments are filled with plagioclase ± fibrolitic sillimanite. Field of view = 2.75 mm. (b) Garnet growth zoning, with slight compositional discontinuity corresponding to the boundary between the inclusion-free and inclusion-filled zones. (c) Fluid inclusion-rich garnet. Note the clear zone around mineral inclusions (biotite, quartz). (d) Fluid inclusion-rich garnet with clear near-rim region. Inclusions are confined to trails arranged in a radial pattern. The greatest concentration of inclusions is adjacent to the inclusion-free/inclusion-filled boundary. Field of view = 1.5 mm. Each photomicrograph is from a different sample.



Fig. 8. Mineral and fluid inclusion-filled garnet (with clear rim) in kyanite. Field of view = 2.75 mm.

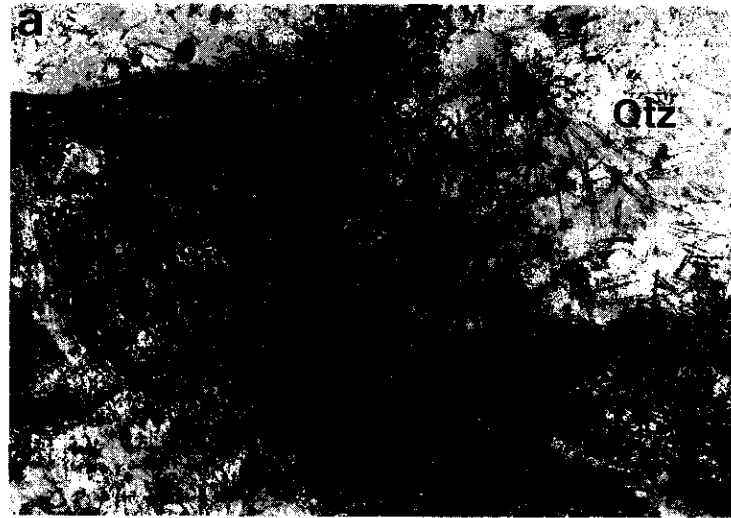
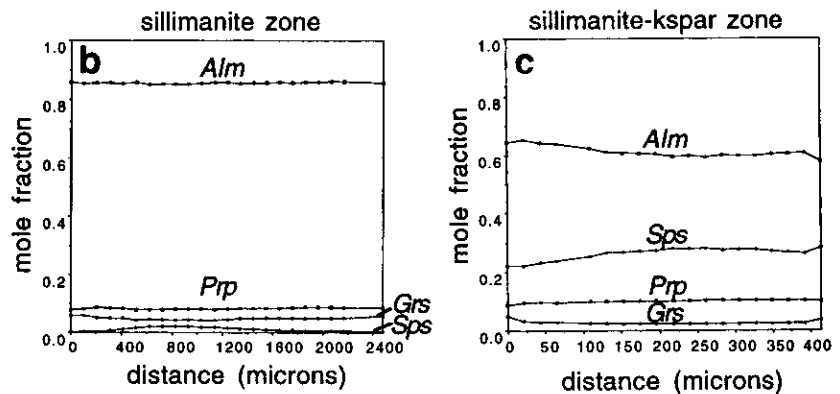


Fig. 9. Sillimanite and sillimanite-K-feldspar zones. (a) Fibrolitic sillimanite is abundant and occurs in randomly orientated sprays and mats in the sillimanite zone. Field of view = 2.75 mm. (b) Garnet zoning in sillimanite zone sample. (c) Garnet zoning in sillimanite-K-feldspar zone rock.



sillimanite occurs in cracks in staurolite. Large muscovite grains contain sprays of fibrolitic sillimanite.

Garnet generally lacks the abundant fluid inclusions present in kyanite zone samples, but some grains contain 100–300 μm -wide bands of small inclusions. These inclusions are too small to determine if they are mineral or fluid inclusions.

Garnet is very almandine-rich ($X_{\text{alm}} = 0.85$; Table 6), with $\text{alm} \gg \text{prp} > \text{grs} > \text{sps}$. Some grains exhibit slight growth zoning, whereas others are homogeneous (Fig. 9b). There is no apparent correlation between degree of zoning and garnet size.

Sillimanite-K-feldspar zone

Coexisting sillimanite and K-feldspar (orthoclase) are found east of the second sillimanite isograd. Muscovite is present in some samples near the isograd, but is absent in the highest grade samples. The sample whose mineral compositions are reported here contains garnet + biotite + muscovite + plagioclase + quartz + K-feldspar + (trace) fibrolitic sillimanite + apatite. Feldspars are the most abundant phases and the rock resembles an orthogneiss, but mineral chemistry suggests the rock may be a metasediment. Garnets in this

sample are similar in composition to garnets in the kyanite zone schist DC93-6. Some grains are slightly zoned, but others are homogeneous (Fig. 9c).

PRESSURE-TEMPERATURE ESTIMATES

Broad estimates of metamorphic conditions for the lowest grade Dutchess County rocks can be obtained from published petrogenetic grids and consideration of the compositions of the minerals. The biotite isograd (see below) probably corresponds to a temperature of 300–400 $^{\circ}\text{C}$; the first appearance of chloritoid in the relatively aluminous rocks probably corresponds to approximately the same temperatures (Spear, 1993).

Pressure-temperature conditions for garnet zone and higher grade rocks were determined using various mineral thermobarometers (Table 8) and petrogenetic grids calculated for Dutchess County mineral compositions using GEOCALC (Fig. 10; Berman *et al.*, 1987). Garnet rim compositions, neighbouring biotite and plagioclase rim compositions were used in one set of calculations; garnet outer core, matrix biotite and plagioclase outer core/core compositions are also reported. In garnet through kyanite zone rocks, the latter compositions yielded higher pressures and tem-

Table 8. Thermobarometric results.

Zone	Assemblage	$T(^{\circ}\text{C})^*$	$P_{\text{GPAQ}}^{\dagger}$ (kbar)	$P_{\text{GPMB}}^{\ddagger}$
Garnet	Rim	435–470		2.1–3.0
	Outer core	475–480		3.2–4.0
Lower St	Rim	450–480		3.7–4.0
	Outer core	505–520		5.5–5.6
Upper St	Rim	485–500		3.0–4.0
	Outer core	512–515		4.3–5.3
Kyanite	Rim	455–525	3.5–4.9 \ddagger	3.8–4.7
	Outer core	450–500	4.5–6.0	3.5–5.2
Sillimanite	Rim	580–590	3.8–4.7	4.6–5.7
	Outer core	585	4.0–5.1	4.4–5.6
Sil-Kfs	Rim	c.720	c.5–6	c.5–6
	Outer core	c.730	c.5–6	c.5–6

* Garnet–biotite geothermometry calibrations of Ferry & Spear (1978) with Berman (1990) garnet solution model and Hodges & Spear (1982) yielded similar results. The range reported represents values obtained from 2–3 garnet–biotite assemblages within the same thin section. \dagger GPAQ = garnet–plagioclase– Al_2SiO_5 –quartz geobarometry (Hodges & Spear, 1982; Koziol & Newton, 1989); GPMB = garnet–plagioclase–muscovite–biotite geobarometry of Ghent & Stout (1981), Hodges & Crowley (1985) and Hoisch (1990). Note: the calibration of Koziol & Newton (1989) consistently yields the highest pressure. \ddagger Fibrolitic sillimanite at garnet rim; note that some kyanite samples (e.g. DC93–4, see Table 5) are very spessartine-rich ($X_{\text{sps}}=0.35$). The thermobarometric results reported include this sample as well as other samples with low X_{sps} .

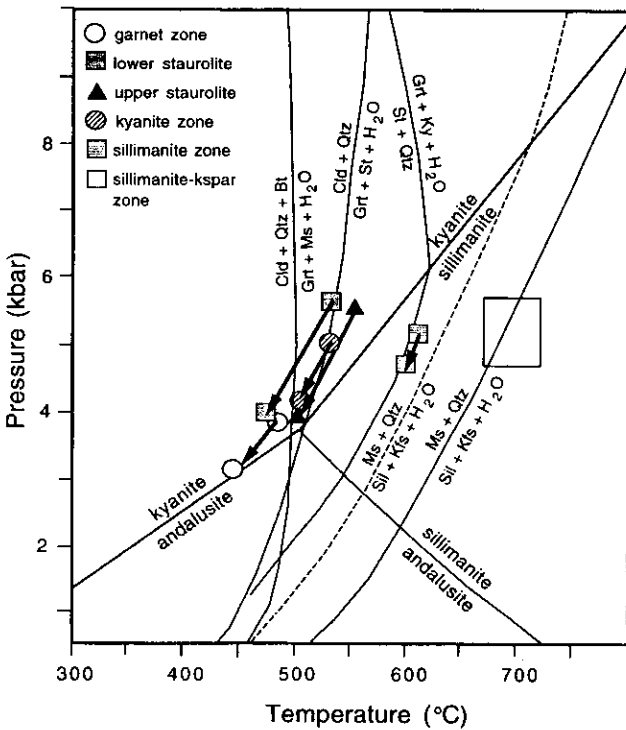
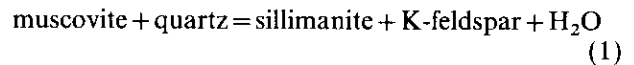


Fig. 10. Petrogenetic grid for Dutchess County rocks. Reactions involving chloritoid and staurolite were calculated using lower staurolite zone mineral compositions. The second sillimanite isograd was calculated at $X_{\text{H}_2\text{O}}=0.5$ (dashed line) and 1.0 (solid line). Approximate P – T conditions for garnet through sillimanite–K-feldspar zone rocks are also indicated. The large box reflects the large uncertainty in P – T calculations for this zone. The arrow between each pair of symbols points from the garnet outer core–matrix assemblage conditions to the garnet rim–adjacent phases conditions.

peratures than those determined using garnet rim and adjacent phases (Table 8, Fig. 10). The P – T conditions recorded by garnet rim composition in staurolite and kyanite zone rocks are essentially the same (450–500 $^{\circ}\text{C}$, c. 4 kbar), perhaps indicating that the thermobarometers closed to further reaction at these conditions. These garnet rim results are similar to those obtained for garnet outer core–matrix assemblages in garnet zone rocks. Some kyanite and most sillimanite zone garnets are essentially unzoned and these samples give similar rim vs. core values for temperature and pressure because there is no difference in composition between matrix biotite and biotite adjacent to garnet, and plagioclase is not strongly zoned.

Thermobarometric calculations for sillimanite–K-feldspar zone samples gave a wide range of results (2–6 kbar) depending on the thermobarometer and calibration used. Application of thermobarometric methods to granulite facies rocks is beset by many problems, such as re-equilibration of minerals on cooling, and P – T results are therefore difficult to interpret. In addition, garnet in these rocks is relatively spessartine-rich ($X_{\text{sps}}=0.27$), and beyond the suggested compositional limits of some calibrations. An estimate of the P – T conditions for the metamorphism of these rocks is obtained from the equilibrium



which is plotted on the petrogenetic grid (Fig. 10) for Dutchess County mineral assemblages and $X_{\text{H}_2\text{O}}=1.0$ and 0.5.

In general, minerals in each successive zone from low to high grade record higher temperatures than the preceding zone. The exception is the kyanite zone, in which garnet outer core and matrix phase compositions record conditions lower than (but similar to) those recorded by staurolite zone rocks.

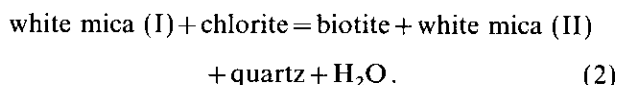
According to the thermobarometric results, temperature increased c. 30 $^{\circ}\text{C}$ and pressure increased <1 kbar from zone to zone (from west to east), with a total difference of c. 300 $^{\circ}\text{C}$ and c. 3 kbar between garnet and sillimanite–K-feldspar zone rocks.

INDEX MINERAL REACTIONS AND REACTION TEXTURES

Metamorphism of the Dutchess County Barrovian sequence is largely the result of Taconic (Ordovician) events that occurred not long after deposition of the protoliths. According to Hames *et al.* (1991), Acadian thermal events may have affected the eastern part of New York state in this region, and Acadian deformation may have extended as far as the Hudson River. The discussion below, however, assumes that major growth of porphyroblasts (i.e. index minerals) occurred during a single metamorphic event.

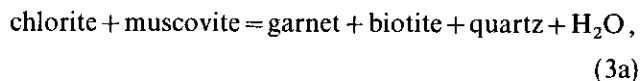
It is not possible to write balanced reactions among Dutchess County samples using analysed mineral compositions. For example, application of the algebraic technique of singular value decomposition (SVD; Fisher, 1989, 1993) for determining possible reaction relations between assemblages failed to determine any mass balance between the analysed chlorite and biotite zone samples. No mass balance relations were identified across any isograds in this sequence, most likely reflecting bulk compositional heterogeneities inherited from the turbiditic protolith and/or metasomatic effects (see below). The reactions given below are therefore model equilibria that explain the observed progression of index minerals across the Barrovian sequence, and, in some case, reaction textures within samples.

Metamorphic minerals in the chlorite zone probably formed from reaction of smectite/illite and other clay minerals. The biotite isograd marks the reaction



In general, white mica (I) is more phengitic than white mica (II, muscovite) formed by equilibrium (2). The analyses in Table 3, however, show that white micas analyzed in both the chlorite and biotite zone samples are phengitic, and in fact the biotite zone sample contains more $\text{FeO}^* + \text{MgO}$ than chlorite zone micas analysed, perhaps because the samples represent different bulk compositions.

In the Dutchess County sequence, the first appearance of garnet is not a function of the bulk composition of the protolith, as the westernmost occurrence of garnet in both pelitic and quartz-rich rocks is in the same compositionally layered outcrop. Garnet core regions are spessartine-rich in graphitic phyllites as well as in quartz-rich rocks, with $X_{\text{sp}} c. 0.25$. The first appearance of garnet in the pelitic rocks was probably the result of the reaction.



or

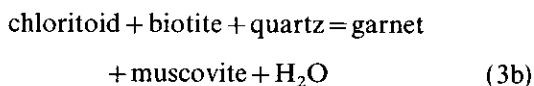


(Fig. 10). Mn-bearing ilmenite may also have been involved in the production of garnet. Wang & Spear (1991) discussed the coexistence of chloritoid + biotite in the Walloomsac Formation north of Dutchess County, and proposed that the occurrence of this assemblage is controlled largely by the bulk composition of the rock. Chloritoid and biotite are predicted to coexist if bulk $\text{Fe}/(\text{Fe} + \text{Mn} + \text{Mg}) > 0.60$ (Wang & Spear, 1991). This is consistent with the bulk composition of the Walloomsac schists in Dutchess County

($X_{\text{Fe}} c. 0.65\text{--}0.81$), and accounts for chloritoid + biotite coexistence in the low-grade rocks.

In garnet zone phyllites, white mica is less phengitic than in the lower grade zones, and plagioclase is more calcic. Carbonate minerals (e.g. ankerite) have only been identified in rocks to the west of the garnet isograd, and are the only major Ca-bearing minerals observed in the low-grade rocks, suggesting that breakdown of ankerite may have contributed to the increase in anorthite component in plagioclase.

Matrix garnet in quartz-rich rocks has been partially resorbed and replaced by a halo of recrystallized quartz (Fig. 3d). As described above, some garnet grains exhibit relict idiomorphic crystal faces; these garnet grains are not surrounded by quartz haloes. Quartz is the only phase present at resorbed garnet rims, suggesting that dissolution of garnet may have been accomplished by action of a fluid that removed components from the rock. Although the matrix of the rock is dominated by fine-grained quartz grains, veins of highly recrystallized quartz can be distinguished by their coarser grain size and may be related to the garnet dissolution event.

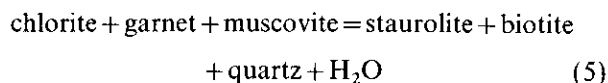
Some garnet in graphitic phyllites also displays dissolution features. Garnet that is cut by quartz veins in the phyllites has been truncated and slightly chemically altered along the garnet-vein contact (Whitney *et al.*, in press). Therefore, although different textures and modal mineralogy are present in the two bulk compositions, both rocks appear to have been influenced by the infiltration of fluid that was largely confined to fractures (veins).

Chloritoid appears in the biotite zone in aluminous bulk compositions, and is observed in less aluminous pelites in the garnet and lower staurolite zones. As described above, garnet in lower staurolite zone phyllites contains ilmenite and chloritoid grains that are partially included in the garnet and bent at the garnet-matrix boundary (Figs 4a & 5b). Although chloritoid appears west of the garnet isograd, and initial growth of chloritoid may pre-date that of garnet, some chloritoid growth clearly post-dated final growth of garnet, as evidenced by the truncation of garnet and garnet growth zoning by chloritoid (Fig. 4c).

In the lower staurolite zone, staurolite has clearly grown at the expense of chloritoid (Fig. 4d), perhaps by an equilibrium such as

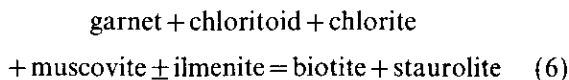


(Fig. 10). Primary chlorite is present in garnet zone rocks and persists into the lower staurolite zone, therefore the equilibrium



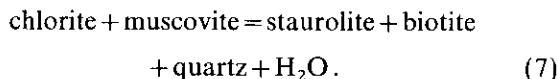
must also be considered. It is important to evaluate both of these reactions, as (4) results in net production of garnet, and (5) results in net consumption of

almandine to produce staurolite (see Spear *et al.*, 1990). If both chlorite and chloritoid are reactants, as seems likely, then



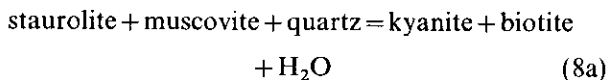
may account for initial growth of staurolite. Local resorption of garnet, particularly in the vicinity of ilmenite (Fig. 4a) may be textural evidence for consumption of garnet by a reaction similar to (6).

Both chloritoid and primary chlorite are absent from the upper staurolite zone. As noted above, large staurolite porphyroblasts contain subidiomorphic garnet inclusions (Fig. 6a); no chemical zoning was detected in garnet or staurolite rim regions to indicate exchange of ferromagnesian components after entrapment of the garnet. Although some included garnet grains lack textural or chemical evidence for dissolution to produce staurolite (equilibria 5 & 6), the inclusions may have experienced late-stage compositional and textural adjustments, and thus have not preserved evidence for reaction. Alternatively, staurolite may have grown largely as a result of breakdown of chloritoid (4), in which garnet was also produced rather than consumed, or by an equilibrium such as



The presence of staurolite inclusions in garnet (near rim regions) and of garnet inclusions in staurolite suggests that both minerals were growing simultaneously during upper staurolite zone metamorphism, perhaps indicating that chlorite was consumed before chloritoid, and that (4) accounts for final garnet and staurolite growth.

Kyanite may have grown at the expense of staurolite, e.g.



or

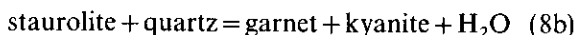
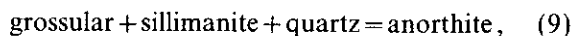


(Fig. 10), although, as in many metapelitic rocks, there is no textural evidence for the kyanite-producing reaction. Although staurolite persists into the lower sillimanite zone (Table 1), it is not observed in most kyanite-bearing schists. Bence & McLelland (1976) attributed this to local variations in bulk composition, and noted that schists lacking staurolite are more Mg-rich than the staurolite-bearing horizons.

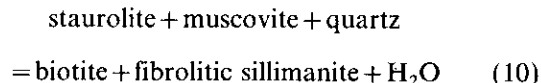
The first appearance of fibrolitic sillimanite coincides with the kyanite isograd (Fig. 1b). In most kyanite zone rocks, fibrolitic sillimanite is texturally late and is associated in some samples with local resorption of garnet by plagioclase (Fig. 7a). Although textures are ambiguous, the presence of randomly orientated clus-

ters of fibrolitic sillimanite along garnet margins where the rim has been embayed by plagioclase suggests that it was produced by a garnet resorption reaction rather than being a reactant, as in the equilibrium



which could take place during decompression and/or heating. Alternatively, fibrolitic sillimanite may have formed by the polymorphic kyanite = sillimanite transformation, but found the garnet-plagioclase contact to be the most favourable place to nucleate, and the presence of the fibrolitic sillimanite in embayments may therefore not be related to resorption of garnet.

As described above, horizons containing large blue kyanite blades, garnet and biotite alternate with more fine-grained layers that lack kyanite but contain abundant fibrolitic sillimanite, plagioclase, quartz, biotite and highly resorbed garnet. Trace elements such as Fe and Mn have not been detected in Dutchess County aluminosilicate phases, and therefore cannot account for local variations in Al_2SiO_5 stability. The variation in the Al_2SiO_5 phase present on an outcrop scale may be evidence that fibrolitic sillimanite nucleation is favoured in some layers as a result of slight differences in bulk composition or response of the rocks to deformation. Bulk compositional variation occurs on an outcrop scale, in part because the protoliths are turbiditic shales and sandstones. If some layers are more Mg-rich than others (see above) and contain staurolite rather than kyanite, fibrolitic sillimanite may have formed preferentially by a reaction involving the breakdown of staurolite, e.g.



that could coincide with the formation of kyanite in adjacent layers. There is, however, no petrographic evidence that staurolite was ever present in the fibrolitic sillimanite-bearing layers. Alternatively, fibrolitic sillimanite growth may post-date kyanite growth not only in the kyanite-bearing layers where there is textural evidence to support this interpretation, but also in the kyanite-absent layers. If some layers are more permeable than others (as a result of structural or lithological heterogeneities), these layers may have been the site of fluid infiltration (see next section), and compositional variation may reflect metasomatic effects. Removal of more soluble elements may have resulted in residual enrichment in Al, and promotion of fibrolitic sillimanite growth during continued high-temperature metamorphism.

The timing of fibrolitic sillimanite growth is unknown. Texturally late fibrolitic sillimanite in kyanite and higher zones may have formed during an increase in temperature and/or pressure decrease subsequent to kyanite growth but during the same metamorphic episode (Taconic), or the fibrolite could represent the

Acadian thermal overprint described by Hames *et al.* (1991).

Relict kyanite and staurolite persist into the lower sillimanite zone, but not in the same rocks. Fibrolitic sillimanite is extremely abundant in some samples, and is typically randomly orientated in large sprays in quartz, plagioclase and muscovite. Whitney *et al.* (in press) speculated that the high fibrolitic sillimanite abundance may be related to metasomatic Al-enrichment. Although outcrops contain quartz and quartz-plagioclase veins, and some garnets contain diffuse trails of abundant, minute inclusions, sillimanite zone garnets do not contain spectacular garnet-vein reaction textures as do the upper staurolite and kyanite zone rocks.

Sillimanite zone samples record slightly lower pressures than preceding zones (Table 8, Fig. 10), but the results are within the uncertainties in the geobarometers (± 1 kbar). It is likely that progression from the kyanite to sillimanite zone involved only a slight increase in pressure. Alternatively, the calculated P - T results may be reflecting modification of garnet compositions by fluid-assisted reactions.

Mineral assemblages in sillimanite-K-feldspar zone rocks reflect the breakdown of muscovite + quartz (1). Although there is some textural evidence for minor retrogression, none of the samples observed in this study contain reaction textures that can be attributed to infiltration of an aqueous fluid. The abundance of feldspars, relative lack of micas and granular texture of the rocks makes them resemble orthogneisses, but the presence of fibrolitic sillimanite and almandine-rich garnet suggests that these rocks are metapelitic gneisses.

Temperatures of *c.* 720 °C are calculated for the Dutchess County sillimanite-K-feldspar zone rocks. The difference between sillimanite zone and sillimanite-K-feldspar zone temperatures is the largest zone-to-zone variation in the sequence. Pressures calculated for the highest grade zone, however, are essentially the same as for the preceding zone.

EVIDENCE FOR FLUID INFILTRATION

Upper staurolite and kyanite zone rocks contain clear evidence for the infiltration of water-rich fluid at elevated temperatures. As described briefly above (and in more detail by Whitney *et al.*, in press), texturally and compositionally distinct zones in garnet along garnet-vein contacts contain abundant fluid inclusions, some of which are confined to trails oriented perpendicular to the trend of the vein (Fig. 6d). Fluid inclusions are also present beyond this reaction zone, but their abundance decreases with distance away from the vein, and no fluid inclusions are present near the garnet rim furthest from the vein (distance from vein *c.* 1.5–2 mm).

In upper staurolite zone rocks, matrix garnet that is not intersected by veins does not contain fluid

inclusions (Fig. 6c), but plagioclase inclusions in these garnets are reverse zoned and surrounded by grossular depletion haloes, suggesting that the core regions of these garnets were open to net transfer reaction during high-grade metamorphism. Fractures must have been present to open garnet interior regions and allow plagioclase inclusions to react, but these have probably healed.

In the kyanite zone, both matrix garnet and garnet inclusions in kyanite contain fluid-inclusion-rich cores and inclusion-free near-rim regions (Figs 7 & 8). Garnet fragments in quartz veins are clouded with abundant fluid inclusions, and matrix garnet cut by veins contains the highest concentrations of fluid inclusions near the garnet-vein contact. The mode of occurrence and distribution of fluid inclusions in garnet varies from sample to sample, and even from garnet to garnet, suggesting local structural control of infiltration on the scale of both the outcrop and the individual garnet grains. Fluid inclusions in some matrix grains are spatially related to adjacent quartz-rich veins, visible and healed microfractures in garnet, and mineral inclusions in garnet (biotite, quartz, ilmenite). Although most mineral inclusions are surrounded by a thin fluid-inclusion-free zone, the region immediately surrounding this clear zone is typically a broad zone of high concentration of fluid inclusions (cf. Hames & Menard, 1993).

Metasomatic reaction textures associated with veining strongly indicate that fluid infiltrated the metapelitic schists along channels (now represented by veins) and triggered high-temperature metasomatic reactions involving garnet and its mineral inclusions, and that the fluid was able to penetrate garnet interiors along microcracks, many of which have subsequently healed. Upper staurolite and kyanite zone rocks contain the most evidence for extensive infiltration and mineral-fluid reaction. These inferences may contradict the proposal of Garlick & Epstein (1967) that the similarity of oxygen isotopic signatures between Dutchess County vein and host rock quartz ($\delta^{18}\text{O}$ *c.* 19‰ in biotite zone; *c.* 13‰ in sillimanite zone) may indicate that vein quartz crystallized from a fluid in isotopic equilibrium with the host metapelites.

Thermobarometric results for kyanite zone rocks are anomalous in the context of the Barrovian sequence (Fig. 10). That is, mineral assemblages record conditions lower than those determined for staurolite zone rocks. The P - T results for staurolite zone assemblages are interpreted to be reasonable because garnet outer core and matrix phase compositions yield garnet-biotite temperatures that are consistent with equilibria describing the first appearance of chloritoid and staurolite (Fig. 10). The kyanite zone mineral assemblages are therefore interpreted to record anomalously low P - T conditions. In addition, although fibrolitic sillimanite locally occurs at garnet rims in kyanite zone samples, the thermobarometric results plot in the kyanite stability field (Fig. 10). Low calculated P - T

results for kyanite zone samples may reflect modification of garnet composition by fluid-assisted reactions, as described above.

Sillimanite–K-feldspar zone rocks are not extensively veined and lack metasomatic features such as those described for the kyanite and upper staurolite zone rocks. This represents a distinct difference from the amphibolite facies rocks in the sequence, and seems to indicate that the granulite facies rocks either did not experience the same infiltration event as the lower grade rocks, or that the response to infiltration was different at $T > 700^\circ\text{C}$ (i.e. infiltration may have triggered partial melting). Calculated values of $a_{\text{H}_2\text{O}}$ determined from phase equilibrium considerations (reaction 1 and paragonite + quartz = albite + sillimanite + H_2O) and following Stout *et al.* (1982) at $T = 700\text{--}720^\circ\text{C}$ and 5–6 kbar range from 0.38 to 0.81, depending on the sample, estimated pressure, temperature and the solution models adopted for micas and feldspars. Comparison of thermobarometric results with the location of equilibrium (1) suggests that a water-rich fluid may have been present.

RELATIVE TIMING OF FLUID INFILTRATION

Veins and microcracks were clearly major conduits for fluid during medium- to high-grade metamorphism. A number of the observations and inferences discussed above provide constraints on the P – T conditions and relative timing of fluid infiltration.

Quartz-rich veins cross-cut and truncate all major minerals in the rock (e.g. garnet, kyanite, staurolite, biotite), and therefore formed subsequent to major porphyroblast growth, but the observations that vein mineralogy varies with metamorphic grade (Vidale, 1974) and that metasomatic reaction occurred along garnet–vein contacts indicate that veins formed during metamorphism at elevated P – T conditions.

Fluid-filled microcracks must also have been present at elevated pressures and temperatures. Fluid inclusions in some garnets are confined to pseudosecondary trails, and these trails are truncated by inclusion-free garnet rims (Figs 7 & 8). Infiltration must have post-dated major garnet growth, but occurred at P – T conditions high enough to allow additional garnet growth/precipitation. The timing of infiltration can therefore be constrained to have occurred between the growth of the garnet outer core and the garnet rim. Combining these textural observations with results of thermobarometric determinations indicates that fluid flow in upper staurolite and kyanite zone rocks probably occurred during decompression at *c.* 4–5 kbar and T *c.* 525–550 $^\circ\text{C}$. Most fluid inclusions in garnet are too small for microthermometric analysis, but a few fluid inclusions located in the garnet outer region that are large enough to permit observation of phase changes on a heating/freezing stage yield densities consistent with trapping at these conditions (Whitney *et al.*, in press). These rocks therefore contain convincing evi-

dence for fluid flow at depth in the crust during metamorphism. Flow was largely channellized, but fluid also infiltrated the rock matrix and grain interiors.

These conclusions are based in part on the assumption that garnet growth occurred during one metamorphic event (Taconic). Although there is strong evidence that the veins formed during Taconic metamorphism and that garnet–fluid metasomatic reaction was related to vein formation (Fig. 6d), there is no unambiguous evidence that all garnet fracturing and infiltration occurred during a single event. If these rocks experienced an Acadian overprint, garnet rims may have grown/reprecipitated during this second metamorphism, and additional fluid-assisted fracturing may have occurred. Even if rim growth occurred during a later metamorphic episode, however, the major infiltration event represented by veins and fluid-inclusion-filled fractures is still constrained to have occurred at elevated P – T conditions by the extent and nature of garnet compositional modification in the vicinity of these features. Work is in progress to obtain isotopic data from garnet core and rim regions to decipher absolute ages for garnet growth and fluid infiltration.

ACKNOWLEDGEMENTS

We thank T. W. Donnelly, J. Walker, T. W. Grover, A. F. Glazner, S. A. Goldberg, and T. J. Bralower for help with this project, and reviews and comments by P. Crowley, M. Brown and an anonymous reviewer. Some samples were collected and kindly provided by T. W. Donnelly.

REFERENCES

- Ague, J. J., 1991. Evidence for major mass transfer and volume strain during regional metamorphism of pelites. *Geology*, **19**, 855–858.
- Balk, R., 1936. Structural and petrological studies in Dutchess County, New York, Part I. Geologic structure of sedimentary rocks. *Geological Society of America Bulletin*, **47**, 685–774.
- Barth, T. F. W., 1936. Structural and petrological studies in Dutchess County, New York, Part II. Petrology and metamorphism of the Paleozoic rocks. *Geological Society of America Bulletin*, **47**, 775–850.
- Bence, A. E. & McLelland, J. M., 1976. Progressive metamorphism in Dutchess County, New York. *New York State Geological Association Guidebook, Trip B-7*.
- Bence, A. E. & Rajamani, V., 1972. $^{40}\text{Ar}/^{39}\text{Ar}$ incremental heating 'ages' of muscovites and biotites from a progressive metamorphic terrain. *Geological Society of America Abstracts with Program*, **449**.
- Berman, R. G., 1990. Mixing properties of Ca–Mg–Fe–Mn garnets. *American Mineralogist*, **75**, 328–344.
- Berman, R., Brown, T. & Perkins, E., 1987. GEOCALC: software for calculation and display of pressure–temperature–composition diagrams. *American Mineralogist*, **72**, 861–862.
- Drake, A. A., Sinha, A. L., Laird, J. & Guy, R. E., 1989. The Taconic Orogen. In: *The Geology of North America, The Appalachian–Ouachita Orogen in the United States* (eds Hatcher, R. D., Thomas, W. A. & Viele, G. W.), *Geological Society of America, Decade of North American Geology series*, **F-2**, 101–178.

- Ferry, J. M. & Spear, F. S., 1978. Experimental calibration of the partitioning of Fe and Mg between biotite and garnet. *Contributions to Mineralogy and Petrology*, **66**, 113–117.
- Fisher, D. W., Isachsen, Y. W. & Rickard, L. V., 1970. Geologic Map of New York, Lower Hudson Sheet. *New York State Museum and Science Service Map and Chart Series*, **15**, scale 1:250 000.
- Fisher, G. W., 1989. Matrix analysis of metamorphic mineral assemblages and reactions. *Contributions to Mineralogy and Petrology*, **102**, 69–77.
- Fisher, G. W., 1993. An improved method of algebraic analysis of metamorphic mineral assemblages. *American Mineralogist*, **78**, 1257–1261.
- Fisher, D. W. & Warthin, A. S., 1976. Stratigraphy and structural geology in western Dutchess County, New York. *New York State Geological Association Guidebook*, **Trip B-6**.
- Garlick, G. D. & Epstein, S., 1967. Oxygen-isotope ratios in coexisting minerals of regionally metamorphosed rocks. *Geochimica et Cosmochimica Acta*, **31**, 181–214.
- Ghent, E. D. & Stout, M. Z., 1981. Geobarometry and geothermometry of plagioclase–biotite–garnet–muscovite assemblages. *Contributions to Mineralogy and Petrology*, **76**, 92–97.
- Hames, W. E. & Menard, T., 1993. Fluid-assisted modification of garnet composition along rims, cracks, and mineral inclusion boundaries in samples of amphibolite facies schists. *American Mineralogist*, **78**, 338–344.
- Hames, W. E., Tracy, R. J., Ratcliffe, N. M. & Sutter, J. F., 1991. Petrologic, structural, and geochronologic characteristics of the Acadian metamorphic overprint on the Taconide zone in part of southwestern New England. *American Journal of Science*, **291**, 887–913.
- Hodges, K. V. & Crowley, P. D., 1985. Error estimation and empirical geothermobarometry for pelitic systems. *American Mineralogist*, **70**, 702–709.
- Hodges, K. V. & Spear, F. S., 1982. Geothermometry, geobarometry, and the Al_2SiO_5 triple point at Mt. Moosilauke, New Hampshire. *American Mineralogist*, **67**, 1118–1134.
- Hoisch, T. D., 1990. Empirical calibration of six geobarometers for the mineral assemblage quartz + muscovite + biotite + plagioclase + garnet. *Contributions to Mineralogy and Petrology*, **104**, 225–234.
- Kozioł, A. M. & Newton, R. C., 1989. Redetermination of the anorthite breakdown reaction and improvement of the plagioclase–garnet– Al_2SiO_5 –quartz barometer. *American Mineralogist*, **73**, 216–223.
- Long, L. E., 1962. Isotopic age study, Dutchess County, New York. *Geological Society of America Bulletin*, **73**, 997–1006.
- McLelland, J. M. & Fisher, D. W., 1976. Stratigraphy and structural geology in the Harlem Valley, S.E. Dutchess County, New York. *New York State Geological Association Guidebook*, **Trip C-7**.
- Ratcliffe, N. M. & Burton, W. C., 1990. Bedrock Geology of the Poughquag Quadrangle, New York. *United States Geological Survey*, **GQ 1662**.
- Spear, F. S., 1993. Metamorphic phase equilibria and pressure–temperature–time paths. *Mineralogical Society of America Monograph*.
- Spear, F. S., Kohn, M. J., Florence, F. P. & Menard, T., 1990. A model for garnet and plagioclase growth in pelitic schists: implications for thermobarometry and P – T path determinations. *Journal of Metamorphic Geology*, **8**, 683–696.
- Stout, M. Z., Crawford, M. L. & Ghent, E. D., 1982. Pressure–temperature and evolution of fluid compositions in Al_2SiO_5 -bearing rocks, Mica Creek, B.C., in light of fluid inclusion data and mineral equilibria. *Contributions to Mineralogy and Petrology*, **92**, 236–247.
- Sutter, J. F., Ratcliffe, N. M. & Mukasa, S. B., 1985. $^{40}\text{Ar}/^{39}\text{Ar}$ and K–Ar data bearing on the metamorphic and tectonic history of western New England. *Geological Society of America Bulletin*, **96**, 123–136.
- Vidale, R. J., 1974. Vein assemblages and metamorphism in Dutchess County, New York. *Geological Society of America Bulletin*, **85**, 303–306.
- Wang, P. & Spear, F. S., 1991. A field and theoretical analysis of garnet + chlorite + chloritoid + biotite assemblages from the tri-state (MA, CT, NY) area, USA. *Contributions to Mineralogy and Petrology*, **106**, 217–235.
- Whitney, D. L., 1991. Calcium depletion halos and Fe–Mn–Mg zoning around faceted plagioclase inclusions in garnet from a high-grade pelitic gneiss. *American Mineralogist*, **76**, 493–501.
- Whitney, D. L., Mechum, T. A. & Dilek, Y. R., in press. Modification of garnet by fluid infiltration during regional metamorphism in garnet through sillimanite zone rocks. *American Mineralogist*.

Received 16 May 1995; revision accepted 9 September 1995.



ILLiad TN: 67853

Borrower: NJM

Lending String: *MDY,XLM,UND,MNN,IBS

Patron: 75 GORRING

Journal Title: Journal of metamorphic geology.

Volume: 14 **Issue:**

Month/Year: 1996**Pages:** 163-81

Article Author:

Article Title: PROGRESSIVE METAMORPHISM
OF PELITIC ROCKS..

Imprint: Oxford ; Boston ; Blackwell Scientific P

ILL Number: 380508



10/24/2003 12:51:47 PM

Call #: Bound Periodicals QE420
.J65

Location: Armstrong Per (Bi Hall)

ARIEL

Charge

Maxcost: Reciprocal/LVIS/\$10IFM

Shipping Address:

Harry A. Sprague Library - ILL
Montclair State University
Upper Montclair, NJ 07043

Fax: 973-655-7780

Ariel: 130.68.120.49